We are IntechOpen, the world's leading publisher of Open Access books Built by scientists, for scientists

4,800
Open access books available

122,000
International authors and editors

135M
Downloads

Our authors are among the

154
Countries delivered to

TOP 1%
most cited scientists

12.2%
Contributors from top 500 universities

CLARIVATE ANALYTICS BOOK CITATION INDEX INDEXED

WEB OF SCIENCE™

Selection of our books indexed in the Book Citation Index in Web of Science™ Core Collection (BKCI)

Interested in publishing with us?
Contact book.department@intechopen.com

Numbers displayed above are based on latest data collected.
For more information visit www.intechopen.com

5

Laser-Driven Table-Top X-Ray FEL

Kazuhisa Nakajima[1,2,3] et al.[*]
[1]*Shanghai Institute of Optics and Fine Mechanics, Chinese Academy of Sciences, Shanghai,*
[2]*High Energy Accelerator Research Organization, Tsukuba,*
[3]*Shanghai Jiao Tong University, Shanghai,*
[1,3]*China*
[2]*Japan*

1. Introduction

Synchrotron radiation sources nowadays benefit a wide range of fundamental sciences - from physics and chemistry to material science and life sciences as a result of a dramatic increase in the brilliance of photons emitted by relativistic electrons when bent in the magnetic field of synchrotron accelerators. A trend will tend toward the X-ray free electron laser (FEL) that will produce high-intensity ultrashort coherent X-ray radiations with unprecedented brilliance as kilometer-scale linear accelerator-based FELs are being commissioned to explore new research area that is inaccessible to date, for instance femtosecond dynamic process of chemical reactions, materials and biomolecules at the atomic level (Gerstner, 2011). Such large-scale tool could be built on a table top if high-quality electrons with small energy spread and divergence are accelerated up to the GeV range in a centimetre-scale length (Grüner et al., 2007; Nakajima et al., 1996; Nakajima, 2008, 2011). It is prospectively conceived that a compact source producing high-energy high-quality electron beams from laser plasma accelerators (LPAs) will provide an essential tool for many applications, such as THz and X-ray synchrotron radiation sources and a unique medical therapy as well as inherent high-energy accelerators for fundamental sciences (Malka et al., 2008).

The present achievements of the laser wakefield accelerator performance on the beam properties such as GeV-class energy (Leemans et al., 2006; Clayton et al., 2010; Lu et al., 2011), 1%-level energy spread (Kameshima et al., 2008; Rechatin et al., 2009), a few mm-

[*]Aihua Deng[1], Hitoshi Yoshitama[4], Nasr A. M. Hafz[3], Haiyang Lu[1], Baifei Shen[1], Jiansheng Liu[1], Ruxin Li[1] and Zhizhan Xu[1]
[1]*Shanghai Institute of Optics and Fine Mechanics, Chinese Academy of Sciences, Shanghai,*
[2]*High Energy Accelerator Research Organization, Tsukuba,*
[3]*Shanghai Jiao Tong University, Shanghai,*
[4]*Hiroshima Unversity, Higashi Hiroshima,*
[1,3]*China*
[2,4]*Japan*

mrad emittance (Karsch et al., 2007), 1-fs-level bunch with a 3-4 kA peak current (Lundh et al., 2011), and good stability and controllability (Hafz et al., 2008; Osterhoff et al., 2008) of the beam production allow us to downsize a large-scale X-ray synchrotron radiation source and FEL to a table-top scale including laser drivers and radiation shields. The undulator radiation from laser-plasma accelerated electron beams has been first demonstrated at the wavelength of $\lambda_{\mathrm{rad}} = 740$ nm and the estimated peak brilliance of the order of 6.5×10^{16} photons/s/mrad²/mm² /0.1% bandwidth driven by the electron beam from a 2-mm-gas jet with the beam energy $E_b = 64$ MeV , the relative energy spread $\Delta E / E_b = 5.5\%$ (FWHM) and total charge $Q_b = 28$ pC , which is produced by a 5 TW 85 fs laser pulse at the plasma density $n_p = 2 \times 10^{19}$ cm^{-3} (Schlenvoigt, 2008). The soft X-ray undulator radiation has been also successfully demonstrated at the wavelength $\lambda_{\mathrm{rad}} = 18$ nm and the estimated peak brilliance of the order of 1.3×10^{17} photons/s/mrad²/mm²/0.1% bandwidth radiated by electrons with $E_b = 207$ MeV , $\Delta E / E_b = 6\%$ (FWHM) and $Q_b = 30$ pC from a 15-mm-hydrogen-fill gas cell driven by a 20 TW 37 fs laser pulse at $n_p = 8 \times 10^{18}$ cm^{-3} (Fuchs, 2009). With extremely small energy spread and peak current high enough to generate self-amplified spontaneous emission so-called SASE (Bonifacio, 1984), a photon flux of the undulator radiation can be amplified by several orders of magnitude to levels of brilliance comparable to current large-scale X-ray FELs (Nakajima, 2008).

Here we consider feasibility of a compact hard X-ray FEL capable of reaching a wavelength of $\lambda_X = 0.1$ nm , which requires the electron beam energy of the multi-GeV range in case of a modest undulator period of the order of a few centimeters. One of prominent features of laser-plasma accelerators is to produce 1-fs-level bunch duration, which is unreachable by means of the conventional accelerator technologies. The X-ray FELs rely on SASE, where the coherent radiation builds up in a single pass from the spontaneous (incoherent) undulator radiation. In an undulator the radiation field interacts with electrons snaking their way when overtaking them so that electrons are resonantly modulated into small groups (micro-bunches) separated by a radiation wavelength and emit coherent radiation with a wavelength equal to the micro-bunch period length. This process requires an extremely high-current beam with small energy spread and emittance in addition to a long precisely manufactured undulator. Therefore the conventional accelerator-based FELs need a long section of the multi-stage bunch compressor called as a 'chicane' that compresses a bunch from an initial bunch length of a few picoseconds to the order of 100 fs to increase the current density of the electron beam up to the order of kilo-ampere level before injected to the undulator, whereas the laser-plasma accelerator based FELs would have no need of any bunch compressor. Although the present LPAs need further improvements in the beam properties such as energy, current, qualities and operating stability, the beam current of 100 kA level (i.e. 100 pC electron charge within 1 fs bunch duration) allows a drastic reduction to the undulator length of several meters for reaching the saturation of the FEL amplification. In addition to inherently compact laser and plasma accelerator, a whole FEL system will be operational on the table-top scale. The realization of laser-driven compact table-top X-ray FELs will benefit science and industry over a broad range by providing new tools enabling the leading-edge research in small facilities, such as universities and hospitals.

2. Laser-plasma accelerators

2.1 Laser wakefields in the linear regime

In underdense plasma an ultraintense laser pulse excites a large-amplitude plasma wave with frequency

$$\omega_p = \sqrt{\frac{4\pi e^2 n_p}{m}} \tag{1}$$

and electric field of the order of

$$E_0 = \frac{mc\omega_p}{e} \simeq 96\left[\mathrm{GV/m}\right]\sqrt{\frac{n_p}{10^{18}\left[\mathrm{cm}^{-3}\right]}} \tag{2}$$

for the electron rest energy mc^2 and plasma density n_p due to the ponderomotive force expelling plasma electrons out of the laser pulse and the space charge force of immovable plasma ions restoring expelled electrons on the back of the ion column remaining behind the laser pulse. Since the phase velocity of the plasma wave is approximately equal to the group velocity of the laser pulse

$$\frac{v_p}{c} \simeq \sqrt{1-\frac{\omega_p^2}{\omega_L^2}} \sim 1 \tag{3}$$

for the laser frequency ω_L and the accelerating field of ~ 100 GV/m for the plasma density ~ 10^{18} cm^{-3}, electrons trapped into the plasma wave are likely to be accelerated up to ~ 1 GeV energy in a 1-cm plasma. In the linear and quasilinear regime with the normalized laser intensity

$$a_0 = \left(\frac{2e^2\lambda_L^2 I_L}{\pi m^2 c^5}\right)^{1/2} \simeq 0.855\times 10^{-9} I_L^{1/2}\left[\mathrm{W/cm}^2\right]\lambda_L\left[\mu\mathrm{m}\right] \sim 1 \tag{4}$$

where I_L is the laser intensity and $\lambda_L = 2\pi c/\omega_L$ is the laser wavelength, the wake potential Φ is obtained from a simple-harmonic equation (Esarey et al., 1996)

$$\frac{\partial^2\Phi}{\partial\zeta^2} + k_p^2\Phi = \frac{1}{2}k_p^2 mc^2 a^2\left(r,\zeta\right) \tag{5}$$

where $\zeta = z - v_p t$, $k_p = \omega_p/c$ and $a\left(r,\zeta\right) \equiv eA\left(r,\zeta\right)/mc^2$ is the normalized vector potential of the laser pulse. The wake potential is given by

$$\Phi\left(r,\zeta\right) = -\frac{m_e c^2 k_p}{2}\int_{\varsigma}^{\infty} d\zeta' \sin k_p\left(\zeta-\zeta'\right)a^2\left(r,\zeta'\right) \tag{6}$$

Thus the axial and radial electric fields are calculated by

$$eE_z = -\frac{\partial \Phi}{\partial z}, \text{ and } eE_r = -\frac{\partial \Phi}{\partial r} \tag{7}$$

Considering a temporally Gaussian laser pulse with $1/e$ half-width σ_L, of which the ponderomotive potential is given by

$$a^2(r,\zeta) = U(r)\exp\left(-\frac{\zeta^2}{\sigma_L^2}\right) \tag{8}$$

the wake potential is

$$\Phi(r,\zeta) = -\frac{\sqrt{\pi}mc^2 k_p \sigma_L}{4} U(r)\exp\left(-\frac{k_p^2\sigma_L^2}{4}\right)\left[C(\zeta)\sin k_p\zeta + S(\zeta)\cos k_p\zeta\right] \tag{9}$$

where $C(\zeta)$ and $S(\zeta)$ are defined as

$$C(\zeta) = 1 - \Re\left[\operatorname{erf}\left(\frac{\zeta}{\sigma_L} - i\frac{k_p\sigma_L}{2}\right)\right], \tag{10}$$

and

$$S(\zeta) = \Im\left[\operatorname{erf}\left(\frac{\zeta}{\sigma_L} - i\frac{k_p\sigma_L}{2}\right)\right], \tag{11}$$

respectively, and

$$\operatorname{erf}(z) = \frac{2}{\sqrt{\pi}}\int_0^z e^{-z'^2} dz' \tag{12}$$

is the complex error function. Using Eq. (7), the axial and radial electric fields are

$$eE_z(r,\zeta) = \frac{\sqrt{\pi}mc^2 k_p^2 \sigma_z}{4} U(r)\exp\left(-\frac{k_p^2\sigma_L^2}{4}\right)\left[C(\zeta)\cos k_p\zeta - S(\zeta)\sin k_p\zeta\right], \tag{13}$$

and

$$eE_r(r,\zeta) = \frac{\sqrt{\pi}mc^2 k_p \sigma_L}{4}\frac{\partial U(r)}{\partial r}\exp\left(-\frac{k_p^2\sigma_L^2}{4}\right)\left[C(\zeta)\sin k_p\zeta + S(\zeta)\cos k_p\zeta\right], \tag{14}$$

respectively. Behind the laser pulse at $\zeta \ll -\sigma_L$, taking into account $C(\zeta) \to 2$ and $S(\zeta) \to 0$, the wakefields are approximately given by

$$eE_z(r,\zeta) \simeq \frac{\sqrt{\pi}m_e c^2 k_p^2 \sigma_L}{2} U(r)\exp\left(-\frac{k_p^2\sigma_L^2}{4}\right)\cos k_p\zeta, \tag{15}$$

and

$$eE_r(r,\zeta) \simeq \frac{\sqrt{\pi} m_e c^2 k_p \sigma_L}{2} \frac{\partial U(r)}{\partial r} \exp\left(-\frac{k_p^2 \sigma_L^2}{4}\right) \sin k_p \zeta \tag{16}$$

For $k_p \sigma_L = \sqrt{2}$, the maximum amplitude of the axial field becomes

$$|E_z|_{\max} = \sqrt{\frac{\pi}{2}} U(0) e^{-\frac{1}{2}} \left(\frac{mc\omega_p}{e}\right) \simeq 0.76 E_0 U(0) . \tag{17}$$

As shown in Eq. (15) and (16), the radial electric field shifts a phase by $\pi/2$ with respect to the axial field and radial dependence of the wakefields is determined by the radial component $U(r)$ of the ponderomotive potential. For a Gaussian laser pulse with linear polarization, the ponderomotive potential is given by

$$a^2(r,z,t) = \frac{a_0^2}{2} \frac{r_L^2}{w^2} \exp\left[-\frac{2r^2}{w^2} - \frac{\left(z - v_p t\right)^2}{\sigma_L^2}\right], \tag{18}$$

where r_L is the laser spot radius at focus, $w = r_L \sqrt{1 + z^2 / z_R^2}$ is the spot radius at z and $z_R = \pi r_L^2 / \lambda_L$ is the Rayleigh length for the laser wavelength λ_L . Assuming that the laser pulse propagates the plasma at a constant spot size $w = r_L$ in a matched plasma waveguide, the ponderomotive potential of the Gaussian mode is

$$a^2(r,\zeta) = \frac{a_0^2}{2} \exp\left(-\frac{2r^2}{r_L^2} - \frac{\zeta^2}{\sigma_L^2}\right) \tag{19}$$

Thus the normalized radial potential is defined as

$$U(r) = \frac{a_0^2}{2} \exp\left(-\frac{2r^2}{r_L^2}\right). \tag{20}$$

For the Gaussian mode, the axial and radial fields Eq. (15) and (16) are

$$eE_z(r,\zeta) = \frac{\sqrt{\pi}}{4} a_0^2 mc^2 k_p^2 \sigma_L \exp\left(-\frac{2r^2}{r_L^2} - \frac{k_p^2 \sigma_L^2}{4}\right) \cos k_p \zeta , \tag{21}$$

and

$$eE_r(r,\zeta) = -\sqrt{\pi} a_0^2 mc^2 k_p \sigma_L \frac{r}{r_L^2} \exp\left(-\frac{2r^2}{r_L^2} - \frac{k_p^2 \sigma_L^2}{4}\right) \sin k_p \zeta . \tag{22}$$

For a Gaussian pulse, the maximum accelerating field is

$$E_{z\max} = \frac{1}{2}\sqrt{\frac{\pi}{2}} e^{-\frac{1}{2}} a_0^2 E_0 \simeq 0.38 a_0^2 E_0 \text{ at } r = 0 \text{ for } k_p \sigma_L = \sqrt{2}\,, \tag{23}$$

and the maximum radial field is

$$E_{r\max} = \sqrt{\frac{\pi}{2}} \frac{e^{-1}}{k_p r_L} a_0^2 E_0 \simeq \frac{0.46}{k_p r_L} a_0^2 E_0 \text{ at } r = \frac{r_L}{2} \text{ for } k_p \sigma_L = \sqrt{2}\,. \tag{24}$$

Consider the radial potential profile described by super-Gaussian functions as

$$U(r) = \frac{a_0^2}{2} \exp\left[-2\left(\frac{r}{r_L} \right)^n \right], \tag{25}$$

where $n \geq 2$ (Sverto, 1998). A Gaussian profile corresponds to $n = 2$. Substituting Eq. (25) into Eq. (15) and (16), the axial and radial wakefieds for a super-Gaussian potential are

$$eE_z(r,\zeta) = \frac{\sqrt{\pi}}{4} a_0^2 m_e c^2 k_p^2 \sigma_z \exp\left[-2\left(\frac{r}{r_L} \right)^n - \frac{k_p^2 \sigma_z^2}{4} \right] \cos k_p \zeta\,, \tag{26}$$

and

$$eE_r(r,\zeta) = -\frac{n}{2} \sqrt{\pi} a_0^2 m_e c^2 k_p \sigma_z \frac{r^{n-1}}{r_L^n} \exp\left[-2\left(\frac{r}{r_L} \right)^n - \frac{k_p^2 \sigma_z^2}{4} \right] \sin k_p \zeta\,. \tag{27}$$

The maximum accelerating field $E_{z\max}$ at $r = 0$ is given by Eq. (23) and the maximum radial field is

$$E_{r\max} = \sqrt{\frac{\pi}{2}} n \left(\frac{n-1}{2n} \right)^{\frac{n-1}{n}} \frac{e^{-\frac{3}{2}+\frac{1}{n}}}{k_p r_L} a_0^2 E_0 \text{ at } \frac{r}{r_L} = \left(\frac{n-1}{2n} \right)^{1/n} \text{ for } k_p \sigma_L = \sqrt{2}\,. \tag{28}$$

The peak laser power with the normalized vector potential a_0 is calculated as

$$P_L = \left(\frac{1}{2} \right)^{2/n} \Gamma\left(\frac{n+2}{n} \right) \frac{(k_L r_L a_0)^2}{8} \left(\frac{m^2 c^5}{e^2} \right) \simeq 8.7[\text{GW}] \left(\frac{1}{2} \right)^{2/n} \Gamma\left(\frac{n+2}{n} \right) \frac{(k_L r_L a_0)^2}{8}, \tag{29}$$

where $k_L = 2\pi/\lambda_L$ is the laser wave number and $\Gamma(z)$ is the Gamma function. For a Gaussian pulse $n = 2$, the peak power is calculated as

$$P_L = \frac{(k_L r_L a_0)^2}{16} \left(\frac{m^2 c^5}{e^2} \right) \simeq 0.544[\text{GW}] (k_L r_L a_0)^2\,, \tag{30}$$

and for a super-Gaussian pulse $n = 4$, the peak power is

$$P_L = \sqrt{\frac{\pi}{2}} \frac{\left(k_L r_L a_0\right)^2}{16} \left(\frac{m^2 c^5}{e^2} \right) \simeq 0.681[\mathrm{GW}] \left(k_L r_L a_0\right)^2 . \tag{31}$$

2.2 Electron acceleration in the quasilinear wakefield

In Eq. (21), for a given plasma density, the maximum field is $E_{z\max} \approx 0.38 a_0^2 E_0$ at the resonant condition $k_p \sigma_L = \sqrt{2}$, while for a given pulse duration, the maximum field is $E_{z\max} \approx 0.33 a_0^2 E_0$ at the resonant condition $k_p \sigma_L = 2$. Changing both plasma density and laser pulse duration, the optimum condition turns out $k_p \sigma_L = 1$ i. e. the FWHM pulse length

$$c\tau_L = 2\sqrt{\ln 2}\,\sigma_L \approx 0.265 \lambda_p , \tag{32}$$

for which the maximum field is

$$E_{z\max} \approx 0.35 a_0^2 E_0 \simeq 10.6[\mathrm{GV/m}] a_0^2 \left(\frac{n_p}{10^{17}\left[\mathrm{cm}^{-3}\right]} \right)^{1/2} . \tag{33}$$

In this condition, the laser pulse length is shorter enough than a half plasma wavelength so that a transverse field at the tail of the laser pulse is negligible in the accelerating phase of the first wakefield. The net accelerating field E_z that accelerates the bunch containing the charge $Q_b = eN_b$, where N_b is the number of electrons in the bunch, is determined by the beam loading that means the energy absorbed per unit length,

$$Q_b E_z = \frac{mc^2 k_p^2 \sigma_r^2}{4 r_e} \frac{E_{z\max}^2}{E_0^2} \left(1 - \frac{E_z^2}{E_{z\max}^2} \right). \tag{34}$$

where $r_e = e^2 / mc^2$ is the classical electron radius and

$$1 - \frac{E_z^2}{E_{z\max}^2} \equiv \eta_b \tag{35}$$

is the beam loading efficiency that is the fraction of the plasma wave energy absorbed by particles of the bunch with the rms radius $\sigma_{r.}$ In the beam-loaded field $E_z = \sqrt{1-\eta_b} E_{z\max}$, the loaded charge is given by

$$Q_b \simeq \frac{e}{4 k_L r_e} \frac{\eta_b k_p^2 \sigma_r^2}{1-\eta_b} \frac{E_z}{E_0} \left(\frac{n_c}{n_e} \right)^{1/2} \approx 232[\mathrm{pC}] \frac{\eta_b k_p^2 \sigma_r^2}{1-\eta_b} \frac{E_z}{E_0} \left(\frac{n_p}{10^{17}\left[\mathrm{cm}^{-3}\right]} \right)^{-1/2} , \tag{36}$$

where $n_c = m\omega_L^2 / 4\pi e^2 = \pi / \left(r_e \lambda_L^2 \right)$ is the critical plasma density and $E_z / E_0 \simeq 0.35 a_0^2 \sqrt{1-\eta_b}$ for $k_p \sigma_L = 1$. Since the loaded charge depends on the accelerating field and the bunch radius, it will be determined by considering the required accelerating gradient and the transverse beam dynamics.

The electron linac with 10 GeV-class beam energy can be composed of a high-quality beam injection stage with beam energy of the order of 100 MeV in a mm-scale length and a high-gradient acceleration stage with meter-scale length. Ideally, the stage length L_{stage} is limited by the pump depletion length L_{pd} for which the total field energy is equal to half the initial laser energy. For a Gaussian laser pulse with the pulse length $k_p\sigma_L = 1$, the pump depletion length is given by

$$k_p L_{\mathrm{pd}} \simeq \frac{8}{\sqrt{\pi}a_0^2 k_p\sigma_L}\frac{\omega_L^2}{\omega_p^2}\exp\left(\frac{k_p^2\sigma_L^2}{2}\right) \approx \frac{7.4}{a_0^2}\frac{n_c}{n_e}. \tag{37}$$

In laser wakefield accelerators, accelerated electrons eventually overrun the acceleration phase to the deceleration phase, of which the velocity is roughly equal to the group velocity of the laser pulse. In the linear wakefield regime, the dephasing length L_{dp} where the electrons undergo both focusing and acceleration is approximately given by

$$k_p L_{\mathrm{dp}} \simeq \pi\frac{\omega_L^2}{\omega_p^2} = \pi\frac{n_c}{n_p} \tag{38}$$

In the condition for the dephasing length less than the pump depletion length $L_{\mathrm{dp}} \le L_{\mathrm{pd}}$, the normalized vector potential should be $a_0 \le 1.5$. Setting $a_0 = \sqrt{2}$, the maximum accelerating field is $E_{z\max} \approx 0.7E_0$ for $k_p\sigma_L = 1$. Assuming the beam-loaded efficiency $\eta_b = 0.5$, the net accelerating field becomes

$$E_z \approx \frac{E_{z\max}}{\sqrt{2}} \simeq 0.5E_0 \approx 15\left[\mathrm{GV/m}\right]\left(\frac{n_p}{10^{17}\left[\mathrm{cm}^{-3}\right]}\right)^{1/2}. \tag{39}$$

With the acceleration stage length approximately equal to the dephasing length

$$L_{\mathrm{stage}} \sim L_{\mathrm{dp}} = \frac{\lambda_p}{2}\frac{n_c}{n_p} = \frac{\lambda_L}{2}\left(\frac{n_c}{n_p}\right)^{3/2} \approx 0.92\left[\mathrm{m}\right]\left(\frac{0.8\left[\mu\mathrm{m}\right]}{\lambda_L}\right)^2\left(\frac{10^{17}\left[\mathrm{cm}^{-3}\right]}{n_p}\right)^{3/2}, \tag{40}$$

the energy gain in the acceleration stage is given by

$$W_{\mathrm{acc}} = E_z L_{\mathrm{stage}} = \pi mc^2\frac{E_z}{E_0}\frac{n_c}{n_p} \approx 28\left[\mathrm{GeV}\right]\frac{E_z}{E_0}\frac{10^{17}\left[\mathrm{cm}^{-3}\right]}{n_p}\left(\frac{0.8\left[\mu\mathrm{m}\right]}{\lambda_L}\right)^2. \tag{41}$$

Here we assume the accelerating field E_z keeps constant over the whole stage length $k_p L_{\mathrm{stage}} \sim \pi(n_c / n_p)$. In fact the 2D particle-in-cell simulation shows that the laser pulse undergoes self-focusing at the entrance of the plasma channel and propagates over the stage length with the energy depletion, leading the average amplitude to be $\langle a\rangle / a_0 \approx 1$ (Nakajima et al., 2011). The plasma density will be determined by setting the required beam energy E_b for the FEL injector linac as

$$n_p = \frac{\pi mc^2}{E_b}\frac{E_z}{E_0}n_c \approx 2.8\times 10^{17}\left[\mathrm{cm}^{-3}\right]\frac{E_z}{E_0}\frac{10[\mathrm{GeV}]}{E_b}\left(\frac{0.8[\mu\mathrm{m}]}{\lambda_L}\right)^2 . \tag{42}$$

The required accelerator length is given by

$$L_{\mathrm{stage}} = \frac{\lambda_L}{2}\left(\frac{E_b}{\pi mc^2}\right)^{3/2}\left(\frac{E_z}{E_0}\right)^{-3/2} \approx 0.2[\mathrm{m}]\left(\frac{E_z}{E_0}\right)^{-3/2}\frac{0.8[\mu\mathrm{m}]}{\lambda_L}\left(\frac{E_b}{10[\mathrm{GeV}]}\right)^{3/2} \tag{43}$$

In the operation of the staged LPA, self-focusing of the drive laser and self-injection of plasma electrons should be suppressed to prevent the beam quality from deterioration as much as possible. These requirements can be accomplished by the LPA operation in the quasilinear regime, where the laser spot size is bounded by conditions for avoiding bubble formation,

$$\frac{k_p^2 r_L^2}{4} > \frac{a_0^2}{\sqrt{1+a_0^2/2}}, \tag{44}$$

and strong self-focusing,

$$\frac{P_L}{P_c} = \frac{\left(k_p r_L a_0\right)^2}{32} \le 1, \tag{45}$$

where $P_c = 2\left(m^2c^5/e^2\right)\omega_L^2/\omega_p^2 \simeq 17\left(n_c/n_p\right)[\mathrm{GW}]$ is the critical power for relativistic self-focusing. These conditions put bounds to the spot size

$$2.4 \le k_p r_L \le 4 \ \text{ for } \ a_0 = \sqrt{2} . \tag{46}$$

For a given spot radius

$$r_L = \frac{\lambda_L}{2\pi}k_p r_L\left(\frac{n_c}{n_e}\right)^{1/2} \approx 17[\mu\mathrm{m}]k_p r_L\left(\frac{10^{17}\left[\mathrm{cm}^{-3}\right]}{n_p}\right)^{1/2}, \tag{47}$$

the peak laser power P_L becomes

$$P_L = \frac{\left(k_p r_L a_0\right)^2}{32}P_c = \left(\frac{k_p r_L a_0}{4}\right)^2\frac{m^2c^5}{e^2}\frac{n_c}{n_p} \approx 9.5[\mathrm{TW}]\left(k_p r_L a_0\right)^2\left(\frac{0.8[\mu\mathrm{m}]}{\lambda_L}\right)^2\frac{10^{17}\left[\mathrm{cm}^{-3}\right]}{n_p} . \tag{48}$$

With the FWHM pulse duration τ_L given by

$$\tau_L = 2\sqrt{\ln 2}\,\frac{\sigma_L}{c} = \frac{\sqrt{\ln 2}}{\pi}\frac{\lambda_L}{c}k_p\sigma_L\left(\frac{n_c}{n_p}\right)^{1/2} \simeq 93[\mathrm{fs}]k_p\sigma_L\left(\frac{10^{17}\left[\mathrm{cm}^{-3}\right]}{n_p}\right)^{1/2}, \tag{49}$$

the required laser pulse energy U_L is calculated as

$$U_L = P\tau_L = \frac{\sqrt{\ln 2}}{16\pi}\frac{\lambda_L}{c}\left(\frac{m^2c^5}{e^2}\right)\left(k_p r_L a_0\right)^2 k_p\sigma_L\left(\frac{n_c}{n_e}\right)^{3/2}$$
$$\approx 0.89[\mathrm{J}]\left(k_p r_L a_0\right)^2 k_p\sigma_L\left(\frac{0.8[\mu\mathrm{m}]}{\lambda_L}\right)^2\left(\frac{10^{17}\left[\mathrm{cm}^{-3}\right]}{n_p}\right)^{3/2}. \quad (50)$$

3. Beam dynamics in laser-plasma accelerators

3.1 Betatron oscillation

Beams that undergo strong transverse focusing forces $F_\perp = -mc^2K^2x$ in plasma waves exhibit the betatron oscillation, where x is the transverse amplitude of the betatron oscillation. From the axial and radial fields, Eqs. (21) and (22), driven by the Gaussian pulse , the focusing constant K is given by

$$K^2 \simeq \frac{4k_p^2}{\left(k_p r_L\right)^2}\frac{E_z}{E_0}\left\langle\sin\Psi\right\rangle, \quad (51)$$

where $\left\langle\sin\Psi\right\rangle$ is set to be the average value over the dephasing phase $0 \le \Psi \le \Psi_{\max}$, where $\Psi_{\max}$ is the maximum dephasing phase at the acceleration distance L_{stage} , i.e. $\Psi_{\max} = (\pi/2)\left(L_{\mathrm{stage}}/L_{dp}\right)$. The envelope equation of the rms beam radius σ_r is given by

$$\frac{d^2\sigma_r}{dz^2} + \frac{K^2}{\gamma}\sigma_r - \frac{\varepsilon_{n0}^2}{\gamma^2\sigma_r^3} = 0, \quad (52)$$

where ε_{n0} is the initial normalized emittance (Schachter, 2011). Assuming the beam energy γ is constant, this equation is rewritten as

$$\frac{d^2\sigma_r^2}{dz^2} + \kappa^2\sigma_r^2 = C, \quad (53)$$

where $\kappa = 2K/\sqrt{\gamma}$ is the focusing strength and $C = 2\sigma'^2_{r0} + \kappa^2\sigma_{r0}^2/2 + 2\varepsilon_{n0}^2/\gamma^2\sigma_{r0}^2$ is the constant given by the initial conditions $\sigma'_{r0} = \left(d\sigma_r/dz\right)_{z=0}$ and $\sigma_{r0} = \sigma_r(0)$. Thus the beam envelope is obtained as

$$\sigma_r^2(z) = \frac{C}{\kappa^2} + \frac{1}{\kappa}\sqrt{\frac{C^2}{\kappa^2} - \frac{4\varepsilon_{n0}^2}{\gamma^2}}\sin\left(\kappa z + \phi_0\right), \quad (54)$$

where

$$\tan\phi_0 = \frac{\sigma_{r0}^2 - C/\kappa^2}{2\sigma_{r0}\sigma'_{r0}/\kappa} \quad (55)$$

The beam envelope oscillates around the equilibrium radius $\bar{\sigma}_r = \sqrt{C}/\kappa$ with the wavelength $2\pi/\kappa = \pi/k_\beta$, where $\lambda_\beta = 2\pi/k_\beta$ is the betatron wavelength. For the condition $C/\kappa = 2\varepsilon_{n0}/\gamma$ that leads to $\sigma_{r0}^2 = 2\varepsilon_{n0}/\kappa\gamma$ with $\sigma_{r0}' = 0$, the beam propagates at the matched beam radius

$$\sigma_{rM}^2 = \frac{2\varepsilon_{n0}}{\kappa\gamma} = \frac{\varepsilon_{n0}}{k_\beta\gamma} = \frac{\varepsilon_{n0}}{K\sqrt{\gamma}} \approx \frac{r_L\varepsilon_{n0}}{2\sqrt{\gamma}}\left(\frac{E_z}{E_0}\langle\sin\Psi\rangle\right)^{-1/2} \tag{56}$$

Consider the betatron oscillation in the wakefields given by Eqs. (26) and (27), driven by the super-Gaussian pulse. The focusing force is written as

$$F_r = -2n\frac{r^{n-1}}{r_L^n}\frac{E_z}{E_0}\sin k_p\zeta\ , \tag{57}$$

where E_z is the peak amplitude of the accelerating field. For $r \ll r_L$, the equation of betatron oscillation is given by

$$\frac{d^2x}{dz^2} + \frac{K^2}{\gamma}x^{n-1} = 0\ , \tag{58}$$

where the focusing constant K^2 is

$$K^2 = \frac{2n}{r_L^n}\frac{E_z}{E_0}\langle\sin k_p\zeta\rangle \tag{59}$$

The envelope equation of the rms beam radius σ_r is given by

$$\frac{d^2\sigma_r}{dz^2} + \frac{K^2}{\gamma}\sigma_r^{n-1} - \frac{\varepsilon_{n0}^2}{\gamma^2\sigma_r^3} = 0 \tag{60}$$

Assuming the beam energy γ is constant, Eq. (60) leads to

$$\frac{d^2\sigma_r^2}{dz^2} + \kappa^2\sigma_r^n = C\ , \tag{61}$$

where

$$\kappa^2 \equiv \frac{2K^2}{\gamma}\frac{n+2}{n} = \frac{4(n+2)}{\gamma r_L^n}\frac{E_z}{E_0}\langle\sin k_p\zeta\rangle \tag{62}$$

and

$$C = 2\left(\frac{d\sigma_r}{dz}\right)_{z=0}^2 + \frac{4K^2}{n\gamma}\sigma_{r0}^n + \frac{2\varepsilon_{n0}^2}{\gamma^2\sigma_{r0}^2} \tag{63}$$

With $(d\sigma_r/dz)_{z=0} = 0$, the equilibrium radius is obtained from setting $d^2\sigma_r^2/dz^2 = 0$ as

$$\sigma_{rM}^2 = \left(\frac{\varepsilon_{n0}}{K\sqrt{\gamma}}\right)^{4/n+2} = r_L^{\frac{2n}{n+2}}\left[\frac{\varepsilon_{n0}^2}{2n\gamma}\left(\frac{E_z}{E_0}\right)^{-1}\left\langle \sin k_p\zeta\right\rangle^{-1}\right]^{\frac{2}{n+2}} \tag{64}$$

3.2 Betatron radiation and radiative damping

The synchrotron radiation causes the energy loss of beams and affects the energy spread and transverse emittance via the radiation reaction force. The motion of an electron traveling along z-axis in the accelerating force eE_z and the radial force eE_r from the plasma wave evolves according to

$$\frac{du_x}{cdt} = -K^2 x + \frac{F_x^{\mathrm{RAD}}}{mc^2}, \qquad \frac{du_z}{cdt} = k_p\frac{E_z}{E_0} + \frac{F_z^{\mathrm{RAD}}}{mc^2}, \tag{65}$$

where $\mathbf{F}^{\mathrm{RAD}}$ is the radiation reaction force and $\mathbf{u} = \mathbf{p}/m_e c$ is the normalized electron momentum. The classical radiation reaction force (Jackson, 1999) is given by

$$\frac{\mathbf{F}^{\mathrm{rad}}}{mc\tau_R} = \frac{d}{dt}\left(\gamma\frac{d\mathbf{u}}{dt}\right) + \gamma\mathbf{u}\left[\left(\frac{d\gamma}{dt}\right)^2 - \left(\frac{d\mathbf{u}}{dt}\right)^2\right], \tag{66}$$

where $\gamma = \left(1+u^2\right)^{1/2}$ is the relativistic Lorentz factor of the electron and

$$\tau_R = \frac{2r_e}{3c} \simeq 6.26\times 10^{-24}\left[\mathrm{s}\right] \tag{67}$$

Since the scale length of the radiation reaction $c\tau_R$ is much smaller than that of the betatron motion, assumming that the radiation reaction force is a perturbation and $u_z >> u_x$. the equations of motion Eqs. (65) are approximately written as

$$\frac{du_x}{dt} \simeq -cK^2 x - c^2\tau_R K^2 u_x\left(1+K^2\gamma x^2\right), \frac{du_z}{dt} \simeq \omega_p\frac{E_z}{E_0} - c^2\tau_R K^4\gamma^2 x^2, \frac{dx}{dt} = \frac{cu_x}{\gamma} \simeq c\frac{u_x}{u_z} \tag{68}$$

Finally the particle dynamics is obtained from the following coupled equations,

$$\frac{d^2x}{dt^2} + \left(\frac{\omega_p}{\gamma}\frac{E_z}{E_0} + \tau_R c^2 K^2\right)\frac{dx}{dt} + \frac{c^2K^2}{\gamma}x = 0, \tag{69}$$

and

$$\frac{d\gamma}{dt} = \omega_p\frac{E_z}{E_0} - \tau_R c^2 K^4\gamma^2 x^2. \tag{70}$$

The particle orbit and the energy are obtained from the coupled equations, Eqs. (69) and (70), describing the single particle dynamics, which can be solved numerically for specified focusing and accelerating fields.

The radiative damping rate is defined by the ratio of the radiated power

$$P_s \simeq \frac{2e^2\gamma^2}{3m^2c^3}F_\perp^2 \tag{71}$$

to the electron energy as

$$\nu_\gamma = \frac{P_s}{\gamma m c^2} \simeq \frac{\tau_R \gamma}{m^2 c^2}F_\perp^2 \tag{72}$$

For the betatron oscillation of a matched beam in the plasma wave, the damping rate is given by

$$\nu_\gamma \simeq \frac{1}{2}\gamma\tau_R c^2 K^4 \left\langle x^2 \right\rangle \simeq \gamma\tau_R c^2 K^4 \sigma_{r0}^2 \approx 16\gamma\tau_R\omega_p^2 \frac{\left(k_p\sigma_{r0}\right)^2}{\left(k_p r_L\right)^4}\left(\frac{E_z}{E_0}\right)^2 \left\langle \sin\Psi \right\rangle^2 . \tag{73}$$

where $\left\langle x^2 \right\rangle = 2\sigma_{x0}^2$ is an average over the beam particles. Assuming the damping time is slow compared to the betatron oscillation

$$\frac{\nu_\gamma}{\omega_\beta} = \frac{\nu_\gamma}{ck_\beta} = \nu_\gamma \frac{\sqrt{\gamma}}{cK} = \tau_R \gamma^{\frac{3}{2}} c K^3 \sigma_{r0}^2 = \tau_R \omega_p \gamma^{\frac{3}{2}} \left(\frac{K}{k_p}\right)^3 \left(k_p\sigma_{r0}\right)^2 \ll 1 , \tag{74}$$

and $\omega_p E_z/E_0 \gg \gamma\tau_R c^2 K^2$ the analytical expression for the mean energy and the relative energy spread are obtained by solving Eqs. (69) and (70) with the initial energy γ_0 and the initial energy spread $\sigma_{\gamma 0}$ (Michel et al., 2006),

$$\gamma = \gamma_0 + \omega_p t \frac{E_z}{E_0} + \frac{2}{5}\gamma_0^2 \frac{\nu_\gamma}{\omega_p}\frac{E_0}{E_z}\left[1 - \left(1 + \frac{\omega_p t}{\gamma_0}\frac{E_z}{E_0}\right)^{5/2}\right], \tag{75}$$

and

$$\frac{\sigma_\gamma^2}{\gamma^2} = \frac{\sigma_{\gamma 0}^2}{\gamma_0^2}\left(1 + \frac{E_z}{E_0}\frac{\omega_p t}{\gamma_0}\right)^{-2}\left\{1 + \frac{4}{25}\left(\frac{\nu_\gamma\gamma_0}{\omega_p}\right)^2\left(\frac{\sigma_{\gamma 0}}{\gamma_0}\right)^{-2}\left(\frac{E_z}{E_0}\right)^{-2}\left[1 - \left(1 + \frac{E_z}{E_0}\frac{\omega_p t}{\gamma_0}\right)^{5/2}\right]^2\right\}. \tag{76}$$

For $\left(\omega_p t/\gamma_0\right)\left(E_z/E_0\right) << 1$, Eq. (76) is approximated to

$$\frac{\sigma_\gamma^2}{\gamma^2} \simeq \left(1 - 2\frac{E_z}{E_0}\frac{\omega_p t}{\gamma_0}\right)\left(\frac{\sigma_{\gamma 0}^2}{\gamma_0^2} + \nu_\gamma^2 t^2\right). \tag{77}$$

Initially the energy spread decreases linearly with time due to acceleration and for later times, $t^2 > \sigma_{\gamma 0}^2/\left(\nu_\gamma^2\gamma_0^2\right)$, the energy spread increases due to the radiative effects. The total energy loss due to the synchrotron radiation is given by

$$\Delta\gamma_{\mathrm{RAD}} \simeq \frac{2}{5}\gamma_0^{-\frac{1}{2}}\gamma_f^{\frac{5}{2}}\frac{\nu_\gamma}{\omega_p}\left(\frac{E_z}{E_0}\right)^{-1} \simeq \frac{32}{5}\tau_R\omega_p\gamma_0^{\frac{1}{2}}\gamma_f^{\frac{5}{2}}\frac{E_z}{E_0}\frac{\left(k_p\sigma_{r0}\right)^2}{\left(k_p r_L\right)^4}\left\langle\sin\Psi\right\rangle^2$$
$$\approx 7.2\times10^{-10}\gamma_0^{\frac{1}{2}}\gamma_f^{\frac{5}{2}}\left\langle\sin\Psi\right\rangle^2\frac{E_z}{E_0}\frac{\left(k_p\sigma_{r0}\right)^2}{\left(k_p r_L\right)^4}\left(\frac{n_p}{10^{17}\left[\mathrm{cm}^{-3}\right]}\right)^{1/2}, \tag{78}$$

where γ_f is the final beam energy and

$$\tau_R\omega_p = \frac{2r_e}{3}k_p \approx 1.12\times10^{-10}\left(\frac{n_e}{10^{17}\left[\mathrm{cm}^{-3}\right]}\right)^{1/2}$$

The energy spread at γ_f becomes

$$\frac{\sigma_\gamma^2}{\gamma^2} \simeq \frac{\sigma_{\gamma0}^2}{\gamma_0^2}\left(\frac{\gamma_f}{\gamma_0}\right)^{-2} + \frac{1024}{25}\tau_R^2\omega_p^2\gamma_0\gamma_f^3\frac{\left(k_p\sigma_{r0}\right)^4}{\left(k_p r_L\right)^8}\left(\frac{E_z}{E_0}\right)^2\left\langle\sin\Psi\right\rangle^4. \tag{79}$$

Assuming the first term that means an adiabatic decrease of the energy spread is neglected in comparison with a radiative increase given by the second term, the energy spread leads to

$$\left(\frac{\sigma_\gamma}{\gamma_f}\right)_{\mathrm{RAD}} \simeq \frac{32}{5}\tau_R\omega_p\gamma_0^{\frac{1}{2}}\gamma_f^{\frac{3}{2}}\frac{E_z}{E_0}\frac{\left(k_p\sigma_{r0}\right)^2}{\left(k_p r_L\right)^4}\left\langle\sin\Psi\right\rangle^2$$
$$\approx 7.2\times10^{-10}\gamma_0^{\frac{1}{2}}\gamma_f^{\frac{3}{2}}\left\langle\sin\Psi\right\rangle^2\frac{E_z}{E_0}\frac{\left(k_p\sigma_{r0}\right)^2}{\left(k_p r_L\right)^4}\left(\frac{n_p}{10^{17}\left[\mathrm{cm}^{-3}\right]}\right)^{1/2}. \tag{80}$$

4. Design considerations on a laser-plasma X-ray FEL

4.1 A design example for 6 GeV LPA-driven X-ray FEL

4.1.1 Requirements for emittance and energy spread

The SASE FEL driven by an electron beam with energy γ requires the transverse normalized emittance

$$\varepsilon_n < \gamma\lambda_X, \tag{81}$$

where λ_X is a FEL wavelength of radiation from the undulator with period λ_u,

$$\lambda_X = \frac{\lambda_u}{2\gamma^2}\left(1+\frac{K_u^2}{2}\right), \tag{82}$$

and K_u is the undulator parameter with the magnetic field strength on the undulator axis B_u,

$$K_u = 0.934 \lambda_u [\mathrm{cm}] B_u [\mathrm{T}] . \tag{83}$$

For lasing a hard X-ray region $\lambda_X \approx 0.1$ nm (the photon energy $E_{\mathrm{photon}} = 12.4$ keV) from the undulator of $\lambda_u = 2$ cm with the magnetic field of $B_u = 0.5$ T ($K_u = 0.934$) at the beam energy $E_b = 6$ GeV ($\gamma = 1.2 \times 10^4$), the normalized emittance should be $\varepsilon_n < 1.2$ μm rad . In addition , it is essential for SASE FELs to inject electron beams with a very high peak current of the order of 100 kA. This requirement imposes a charge of ~ 200 pC on the LPA design in the case of accelerated bunch length of 2 fs. Eq. (36) determines the operating plasma density to be $n_p \sim 10^{17}$ cm^{-3} for $k_p \sigma_r = 1$ and $\eta_b \approx 0.5$. The matched beam condition Eq. (56) for a given initial normalized emittance ε_{n0} imposes an allowable linear focusing strength,

$$\begin{aligned} \frac{K}{k_p} &= \frac{2}{k_p r_L}\left(\frac{E_z}{E_0}\right)^{1/2} \sqrt{\langle \sin\Psi \rangle} \le \frac{k_p \varepsilon_{n0}}{k_p^2 \sigma_{r0}^2 \sqrt{\gamma_0}} \\ &\approx 4.25 \times 10^{-3} \frac{1}{k_p^2 \sigma_{r0}^2} \frac{\varepsilon_{n0}}{1[\mu\mathrm{m}]} \left(\frac{100[\mathrm{MeV}]}{E_i}\right)^{1/2} \left(\frac{n_p}{10^{17}\left[\mathrm{cm}^{-3}\right]}\right)^{1/2}, \end{aligned} \tag{84}$$

where E_i is the injection energy. For $k_p \sigma_{r0} = 1$, $E_i = 100$ MeV and $n_p \sim 10^{17}$ cm^{-3} , a given emittance $\varepsilon_{n0} \approx 1 \mu$m rad leads to $K/k_p \le 5 \times 10^{-3}$, which limits the injection phase to be

$$0 \le \Psi_0 \le \sin^{-1}\left[6.25 \times 10^{-6} \left(k_p r_L\right)^2 \left(\frac{E_z}{E_0}\right)^{-1} \right] \tag{85}$$

For $k_p r_L = 3$ and $E_z / E_0 = 0.5$, the injection phase angle should be $0 \le \Psi_0 \le 0.006^\circ$. In the case of the mismatched beam with a finite energy spread, different particles will undergo betatron oscillations at different frequencies, $\omega_\beta \propto \gamma^{-1/2}$, which will lead to decoherence that is a slippage of the particles with respect to each other, and then to emittance growth until the emittance reaches the matched value. This emittance growth rate (Michel et al., 2006) is given by

$$\nu_\varepsilon = \frac{\omega_\beta \sigma_\gamma}{\sqrt{8}\gamma} \simeq \frac{Kc}{\sqrt{8\gamma}} \frac{\sigma_\gamma}{\gamma} . \tag{86}$$

Without the betatron radiation, the evolution of the transverse emittance can be approximately calculated from

$$\varepsilon_n^2 \approx \gamma_0 K^2 \sigma_{r0}^4 \left(1 - e^{-8\nu_\varepsilon^2 t^2}\right). \tag{87}$$

For $8\nu_\varepsilon^2 t^2 \ll 1$,

$$\varepsilon_n \approx 2\sqrt{2}\sigma_{r0}^2 K \gamma_0^{1/2} \nu_\varepsilon t = k_p^2 \sigma_{r0}^2 \left(\frac{K}{k_p}\right)^2 \left(\frac{\gamma_0}{\gamma}\right)^{1/2} \frac{\sigma_\gamma}{\gamma} ct = \frac{4}{k_p}\left(\frac{k_p \sigma_{r0}}{k_p r_L}\right)^2 \left(\frac{\gamma_0}{\gamma}\right)^{1/2} \frac{E_z}{E_0} \frac{\sigma_\gamma}{\gamma} k_p z \sin\Psi , \tag{88}$$

where z is the acceleration distance and $\Psi = k_p\left(z - v_p t\right) + \Psi_0$ is the aceleration phase. Considering the energy spread,

$$\frac{\sigma_\gamma}{\gamma} = \left(\frac{\sigma_\gamma}{\gamma}\right)_0 \frac{\gamma_0}{\gamma}, \text{ and } \gamma = \gamma_0 + k_p z \frac{E_z}{E_0},$$

the normalized emittance becomes

$$\varepsilon_n \approx \frac{4\gamma_0}{k_p}\left(\frac{k_p\sigma_{r0}}{k_p r_L}\right)^2 \left(\frac{\sigma_\gamma}{\gamma}\right)_0 \left(\frac{\gamma_0}{\gamma}\right)^{1/2} \left(1 - \frac{\gamma_0}{\gamma}\right) \sin\Psi . \tag{89}$$

Setting $\varepsilon_n \le \varepsilon_{n0}$ at $z = L_{\text{stage}}$ and $\gamma = \gamma_f$, the initial relative energy spread is limited to

$$\left(\frac{\sigma_\gamma}{\gamma}\right)_{0\text{G}} \le \frac{k_p\varepsilon_{n0}}{4\gamma_0 \sin\Psi_{\max}}\left(\frac{k_p r_L}{k_p\sigma_{r0}}\right)^2 \left(\frac{\gamma_f}{\gamma_0}\right)^{1/2}$$

$$\approx \frac{0.8\times 10^{-4}}{\sin\Psi_{\max}}\left(\frac{k_p r_L}{k_p\sigma_{r0}}\right)^2 \left(\frac{E_b}{E_i}\right)^{1/2} \frac{\varepsilon_{n0}}{1[\mu\text{m}]}\left(\frac{100[\text{MeV}]}{E_i}\right)^{1/2} \left(\frac{n_p}{10^{17}\left[\text{cm}^{-3}\right]}\right)^{1/2} . \tag{90}$$

For $k_p\sigma_{r0} = 1$, $k_p r_L = 3$, $E_b = 6$ GeV and $E_i = 100$ MeV, the allowable energy spread scales as

$$\left(\frac{\sigma_\gamma}{\gamma}\right)_{0\text{G}} \le 5.5\times 10^{-3} \frac{\varepsilon_{n0}}{1[\mu\text{m}]}\left(\frac{n_p}{10^{17}\left[\text{cm}^{-3}\right]}\right)^{1/2} . \tag{91}$$

For the super-Gaussian drive pulse, as the betatron frequency is dependent on the oscillation amplitude as

$$\omega_\beta = ck_\beta = \frac{cK}{\sqrt{\gamma}}\sigma_r^{\frac{n-2}{2}} , \tag{92}$$

with the matched beam radius Eq. (64), the normalized emittance is

$$\varepsilon_{n\text{SG}} \simeq \sigma_{r0}^n K^2 \left(\frac{\gamma_0}{\gamma}\right)^{1/2} \frac{\sigma_\gamma}{\gamma} ct = \frac{2n\gamma_0}{k_p}\left(\frac{k_p\sigma_{r0}}{k_p r_L}\right)^n \left(\frac{\sigma_\gamma}{\gamma}\right)_0 \left(\frac{\gamma_0}{\gamma}\right)^{1/2} \left(1 - \frac{\gamma_0}{\gamma}\right) \sin\Psi . \tag{93}$$

For $n = 2$, Eq. (93) becomes the Gaussian pulse case given by Eq. (89). The allowable energy spread for the super-Gaussian pulse is given by

$$\left(\frac{\sigma_\gamma}{\gamma}\right)_{0\text{SG}} \le \frac{k_p\varepsilon_{n0}}{2n\gamma_0}\left(\frac{k_p r_L}{k_p\sigma_{r0}}\right)^n \left(\frac{\gamma_f}{\gamma_0}\right)^{1/2} \approx \frac{1.52\times 10^{-4}}{n}\left(\frac{k_p r_L}{k_p\sigma_{r0}}\right)^n \left(\frac{E_b}{E_i}\right)^{1/2} \frac{\varepsilon_{n0}}{1[\mu\text{m}]}\left(\frac{100[\text{MeV}]}{E_i}\right)^{1/2} \left(\frac{n_p}{10^{17}\left[\text{cm}^{-3}\right]}\right)^{1/2} \tag{94}$$

For $k_p\sigma_{r0}=1$, $k_p r_L=3$, $E_b=6$ GeV, $E_i=100$ MeV and $n=4$ (6),

$$\left(\frac{\sigma_\gamma}{\gamma}\right)_{0\mathrm{SG}} \le 2\,(13)\times 10^{-2}\,\frac{\varepsilon_{n0}}{1[\mu\mathrm{m}]}\left(\frac{n_p}{10^{17}\left[\mathrm{cm}^{-3}\right]}\right)^{1/2} \tag{95}$$

The super-Gaussian wakefields mitigate the emittance growth due to mismatching of the injected beam.

In order to reach the X-ray wavelength $\lambda_X=0.1$ nm using the undulator with $\lambda_u=2$ cm, the maximum beam energy E_b is set to be 6 GeV. The accelerator stage length becomes $L_{\mathrm{stage}}=0.4\ \mathrm{m}\approx 0.43L_{\mathrm{dp}}$ where the accelerating field is $E_z=15\ \mathrm{GV/m}$ at the operating plasma density $n_p=1\times 10^{17}\ \mathrm{cm}^{-3}$. Setting the injection phase $\Psi_0\simeq 0^\circ$, the acceleration distance corresponds to the dephasing phase

$$0^\circ \le \Psi \le \frac{\pi}{2}\frac{L_{\mathrm{stage}}}{L_{dp}} \approx 39^\circ\left(\frac{\lambda_L}{0.8[\mu\mathrm{m}]}\right)^2\left(\frac{n_p}{10^{17}\left[\mathrm{cm}^{-3}\right]}\right)^{3/2}. \tag{96}$$

Scanning the electron beam energy in the range from 1.2 GeV to 6 GeV can allow the FEL to cover the X-ray wavelengths $0.1\ \mathrm{nm}\le\lambda_X\le 2.5$ nm ($496\ \mathrm{eV}\le E_{\mathrm{photon}}\le 12.4$ keV).

The FEL operation is characterized by the FEL Pierce parameter (Bonifacio, 1984),

$$\rho_{\mathrm{FEL}}=\frac{1}{2\gamma}\left[\frac{I_b}{I_A}\left(\frac{\lambda_u K_u A_u}{2\pi\sigma_r}\right)^2\right]^{1/3}, \tag{97}$$

where I_b is the beam current, $I_A=17$ kA is the Alfven current, σ_r is the r.m.s transverse size of the electron bunch, and the coupling factor is $A_u=1$ for a helical undulator and $A_u=J_0(\xi)-J_1(\xi)$ for a planar undulator, where $\xi=K_u^2/4\left(1+K_u^2/2\right)$ and J_0 and J_1 are the Bessel functions of the first kind. For $\lambda_u=2$ cm, $K_u=0.934$ and $A_u\approx 0.92$, assuming the average beta function in the undulator $\bar{\beta}_u=1$ m, the FEL parameter can be obtained as

$$\rho_{\mathrm{FEL}}\simeq 0.0032\left(\frac{I_b}{100[\mathrm{kA}]}\right)^{1/3}\left(\frac{E_b}{6[\mathrm{GeV}]}\right)^{-2/3}\left(\frac{\varepsilon_n}{1[\mu\mathrm{m}]}\right)^{-1/3}. \tag{98}$$

The gain length L_{gain} that is the *e*-folding length of the exponential amplification of the radiation power is

$$L_{\mathrm{gain}}=\frac{\lambda_u}{2\pi\sqrt{3}\rho_{\mathrm{FEL}}} \tag{99}$$

The saturation length is set to be $L_{\mathrm{sat}}\sim(10-15)L_{\mathrm{gain}}\approx\lambda_u/\rho_{\mathrm{FEL}}$, at which the saturation power is approximately $P_{\mathrm{sat}}\sim\rho_{\mathrm{FEL}}I_bE_b$. Accordingly the spectral band width is

$1/N_u \sim \rho_{\mathrm{FEL}}$, where N_u is the number of undulator periods. Assuming a bunch duration of $\tau_b \approx 2$ fs , the beam current scales as

$$I_b = \frac{Q_b}{\tau_b} \approx 58[\mathrm{kA}]\left(\frac{n_p}{10^{17}\left[\mathrm{cm}^{-3}\right]}\right)^{-1/2}, \tag{100}$$

for $k_p\sigma_r = 1$ and $E_z/E_0 = 0.5$. With $L_{\mathrm{stage}} = 0.4$ m , the beam energy scales as

$$E_b \approx 6[\mathrm{GeV}]\left(\frac{n_p}{10^{17}\left[\mathrm{cm}^{-3}\right]}\right)^{1/2}. \tag{101}$$

The required emittance for SASE FEL is

$$\varepsilon_n \simeq \gamma\lambda_X = \frac{\lambda_u}{2\gamma}\left(1+\frac{K_u^2}{2}\right) \approx 1.2[\mu\mathrm{m}]\left(\frac{n_p}{10^{17}\left[\mathrm{cm}^{-3}\right]}\right)^{-1/2}, \tag{102}$$

for $\lambda_u = 2$ cm , $K_u = 0.934$. Accordingly the FEL parameter scales as

$$\rho_{\mathrm{FEL}} \simeq 0.0025\left(\frac{n_p}{10^{17}\left[\mathrm{cm}^{-3}\right]}\right)^{-1/3}, \tag{103}$$

and the relative energy spread requirement for the SASE FEL is given as

$$\frac{\sigma_\gamma}{\gamma} \le \rho_{\mathrm{FEL}}\,. \tag{104}$$

4.1.2 Numerical studies of betatron radiation effects

According to Eq. (80), we estimate the energy spread growth due to the betatron radiation from the electron beam accelerated in the wakefields from the injection energy $E_i = 100$ MeV ($\gamma_i \simeq 200$) to $E_b = 6$ GeV ($\gamma_f = 1.2\times10^4$) for $E_z/E_0 = 0.5$, $k_p\sigma_{r0} = 1$, $k_p r_L = 3$ and $\langle \sin\Psi \rangle = 1/2$ as

$$\left(\frac{\sigma_\gamma}{\gamma_f}\right)_{\mathrm{RAD}} \approx 2\times10^{-5}\left(\frac{n_p}{10^{17}\left[\mathrm{cm}^{-3}\right]}\right)^{1/2}, \tag{105}$$

which is much smaller than ρ_{FEL} . For avoiding the normalized emittance growth due to the betatron oscillation, setting the initial energy spread $(\sigma_\gamma/\gamma)_0 \approx 1$ % adiabatically decreases to be $(\sigma_\gamma/\gamma)_f \approx 0.02$ % < ρ_{FEL} after accelerated up to 6 GeV.

The degradation of the energy spread and the emittance due to betatron radiation effects is investigated by solving the coupled equations, Eqs. (69) and (70), describing the single

particle dynamics. We have solved them numerically for the case of the aforementioned 6 GeV LPA. Using the numerical results for a set of test particles that can be solved for the initial conditions corresponding to the initial energy, energy spread and transverse emittance, an estimate of the underlying beam parameter can be calculated as an ensemble average over test particles; for example, the mean energy is given by

$$\langle\gamma\rangle = \sum_i \gamma_i / N_p \,, \tag{106}$$

where γ_i is the energy of the i th particle and N_p is the number of test particles, and the energy spread is defined as

$$\sigma_\gamma^2 = \langle\gamma^2\rangle - \langle\gamma\rangle^2 \,. \tag{107}$$

The normalized transverse emittance is calculated as

$$\varepsilon_{nx}^2 = \langle(x-\langle x\rangle)^2\rangle\langle(u_x-\langle u_x\rangle)^2\rangle - \langle(x-\langle x\rangle)(u_x-\langle u_x\rangle)\rangle^2 \,, \tag{108}$$

where $u_x = \gamma dx/cdt$, with averaging over the ensemble of particles. The single particle equations of motion, Eqs. (69) and (70), are integrated numerically using the Runge-Kutta algorithm. We have carried out numerical calculations for an ensemble of $N_p = 10^4$ particles for the parameters of the 6 GeV LPA operated at $n_p = 1\times10^{17}$ cm^{-3} as shown in Table 1.

The results of our numerical calculations are shown in Fig. 1 together with the analytical estimates for $\langle\gamma\rangle$ and $\sigma_\gamma/\langle\gamma\rangle$, calculated from Eqs. (75) and (76). The numerical calculations are in excellent agreement with the analytical expressions. The relative energy spread in the beginning decreases linearly in time due to the linear increase of the zeroth order mean energy. For the numerical calculations the final value is $(\sigma_\gamma/\langle\gamma\rangle)_{\text{numerical}} = 1.7\times10^{-4}$ at the end of the stage, while the analytical estimate calculates $(\sigma_\gamma/\langle\gamma\rangle)_{\text{analytical}} = 1.7\times10^{-4}$. The $\langle\gamma\rangle$ increases almost linearly in time and reaches a final value of 1.2×10^4 for both the analytical and the numerical calculations after the LPA stage, which corresponds to an electron energy of 6 GeV. Since the radiative effects are negligibly small as estimated from Eq. (105), the emittance is well conserved over the LPA stage, where the matched beam is injected. In Fig. 1, an analytical estimate of the emittance evolution is given by

$$\begin{aligned}\Omega(\gamma) = \Omega_0 \exp[-(\frac{\gamma}{\gamma_{\text{ld}}} - \frac{\gamma_0}{\gamma_{\text{ld}}}) - e^{\frac{\gamma_0}{\gamma_{ld}}}[(\frac{\gamma}{\gamma_{\text{nd}}})^{\frac{3}{2}} - (\frac{\gamma_0}{\gamma_{\text{nd}}})^{\frac{3}{2}}]] \\ \{1 + \frac{1}{4\alpha\sqrt{\chi\gamma_0}}(\frac{2\gamma_0}{\gamma_{\text{ld}}} + \frac{3}{\chi}(\frac{\gamma_0}{\gamma_{\text{nd}}})^{\frac{3}{2}})(1 - e^{-4\alpha\chi^{-\frac{1}{2}}(\sqrt{\gamma}-\sqrt{\gamma_0})})\}\end{aligned} \,, \tag{109}$$

where $\Omega(\gamma) = k_p\varepsilon_{nx}$ is the dimensionless normalized emittance at γ , $\Omega_0 = \Omega(\gamma_0)$, $\chi \equiv E_z/E_0$, $K/k_p = \alpha\chi^{1/2}$, γ_{ld} is the linear damping energy, at which the emittance damps to $\Omega/\Omega_0 \sim 1/e$,

$$\gamma_{ld} = \frac{2}{\tau_R \omega_p \alpha^2} = \left(\frac{2\sqrt{\pi}}{3} \alpha^2 r_e^{\frac{3}{2}} \sqrt{n_p} \right)^{-1} \approx 1.8 \times 10^{10} \frac{E_z}{E_0} \left(\frac{K}{k_p} \right)^{-2} \left(\frac{n_p}{10^{17} \left[\mathrm{cm}^{-3} \right]} \right)^{-1/2}, \qquad (110)$$

and γ_{nd} is the nonlinear damping energy, given by

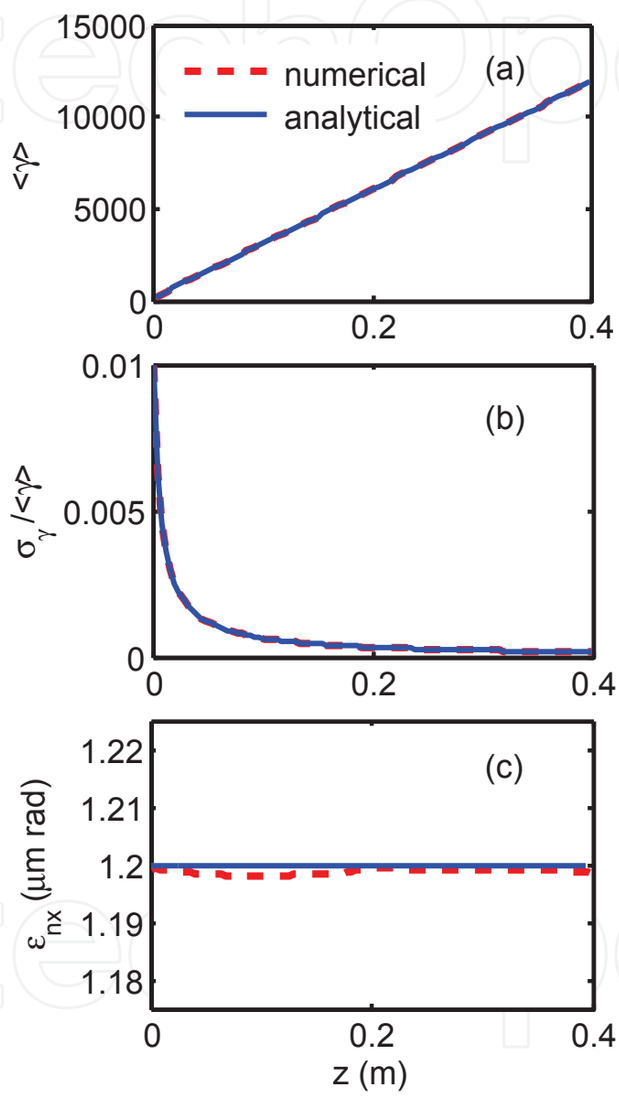

Fig. 1. The results of the beam dynamics calculations for the 6 GeV LPA at the operating plasma density $n_p = 1 \times 10^{17}$ cm^{-3}: (a) mean energy, (b) relative energy spread and (c) normalized transverse emittance over the stage length 0.4 m for the initial energy 100 MeV, initial energy spread of 1%, initial normalized emittance 1.2 μm rad, and constant accelerating field $E_z = 15$ GV/m . The dashed curves show the numerical calculations, while the solid curves show the analytical expressions Eqs. (75) and (76) for mean energy and relative energy spread, and Eq. (109) for normalized emittance, respectively.

$$\gamma_{\mathrm{nd}} \simeq \frac{1}{\alpha^2}\left(\frac{1}{2\tau_R\omega_p\chi^{1/2}\Omega_0}\right)^{2/3} = \frac{1}{\alpha^2\chi^{1/3}}\left(\frac{3}{16\pi r_e^2 n_p\varepsilon_{n0}}\right)^{2/3} \approx 3.84\times10^6\left(\frac{E_z}{E_0}\right)^{-1/3}\left(\frac{K}{k_p}\right)^{-2}\left(\frac{n_p}{10^{18}\left[\mathrm{cm}^{-3}\right]}\frac{\varepsilon_{n0}}{1[\mu\mathrm{m}]}\right)^{-2/3}. \tag{111}$$

For the given parameters $\chi = 0.5$, $\alpha = 0.37$ and $\varepsilon_{n0} = 1.2$ μm rad at $n_p = 10^{17}$ cm^{-3}, the linear damping energy is $\gamma_{\mathrm{ld}} \sim 1.3\times10^{11}$ (66 PeV), while the nonlinear damping energy is $\gamma_{\mathrm{nd}} \sim 1.5\times10^{8}$ (75 TeV).

4.1.3 Attainable peak brilliance of the laser-driven X-ray FEL

In the saturation regime, the photons flux of X-ray radiation is

$$N_{\mathrm{photon}} \approx \rho_{\mathrm{FEL}}\frac{E_b}{E_{\mathrm{photon}}}\frac{I_b}{e} \approx 4.4\times10^{26}\left[\mathrm{s}^{-1}\right] \tag{112}$$

for $E_b = 6$ GeV, $E_{\mathrm{phton}} = 12.4$ keV ($\lambda_X = 0.1$ nm), $\rho_{\mathrm{FEL}} = 0.0025$ and $I_b = 58$ kA. Thus the peak brilliance can be obtained as

$$B_{\mathrm{peak}} = \frac{N\gamma^2}{4\pi^2\varepsilon_n^2}\left(\frac{\Delta\lambda}{\lambda}\right)^{-1} \approx 4.4\times10^{32}\left[\mathrm{photons/s\ mm^2\ mrad^2\ 0.1\%BW}\right]. \tag{113}$$

This peak brilliance is comparable to large-scale X-ray FELs based on the conventional linacs (Ackermann et al., 2007).

The parameters of the required drive laser pulse can be obtained from Eq. (47)-(50) for $a_0 = 1.4$, $k_p\sigma_L = 1$, $k_p r_L = 3$ and $n_p = 1\times10^{17}$ cm^{-3} as follows: the laser spot radius is $r_L = 51$ μm, the peak laser power is $P_L = 171$ TW, the pulse duration is $\tau_L = 93$ fs and the laser pulse energy is $U_L \approx 16$ J at the laser wavelength $\lambda_L = 0.8$ μm. It is necessary for laser-plasma accelerators to propagate ultraintense laser pulses with peak power of the order of 200 TW over the single stage distance of the order of 0.4 m at repetition rate of 10 Hz. Stably propagating laser pulses through the plasma channel with a parabolic density profile

$$n(r) = n_p + \Delta n\frac{r^2}{r_{ch}^2}, \tag{114}$$

where Δn is the density depth at the channel radius r_{ch}, requires that its spot radius r_L should be equal to the matched radius

$$r_{LM} = \left(\frac{r_{ch}^2}{\pi r_e\Delta n}\right)^{1/4}. \tag{115}$$

For this condition, the density depth of plasma channel is given by

$$\frac{\Delta n}{n_p} = \frac{\Delta n_c}{n_p}\left(\frac{r_{ch}}{r_L}\right)^2 = \frac{4}{k_p^2 r_L^2}\left(\frac{r_{ch}}{r_L}\right)^2, \tag{116}$$

where $\Delta n_c = 1/\left(\pi r_e r_L^2\right)$ is the critical channel depth (Sprangle, 1992).

The design parameters of a table-top X-ray FEL driven by the 6 GeV LPA are summarized for a wavelength of $\lambda_X = 0.1$ nm in Table 1.

Electron beam parameters	
Beam energy E_b	6 GeV
Peak beam current I_b	58 kA
Energy spread (rms) σ_γ/γ	0.02%
Pulse duration τ_b	2 fs
Normalized emittance ε_n	1.2 mm mrad
Laser-plasma accelerator parameters	
Plasma density n_p	1×10^{17} cm^{-3}
Plasma wavelength λ_p	106 μm
Channel depth at r_L $\Delta n_c/n_p$	0.44
Accelerating field E_z	15 GV/m
Injection beam energy E_i	100 MeV
Stage length L_{stage}	40 cm
Charge per bunch Q_b	116 pC
Laser wavelength λ_L	0.8 μm
Normalized laser intensity a_0	1.4
Laser pulse duration τ_L	93 fs
Laser spot radius r_L	51 μm
Laser peak power P_L	171 TW
Laser pulse energy U_L	16 J
Undulator parameters	
Undulator period λ_u	2 cm
Undulator parameter K_u	0.934
FEL parameter ρ_{FEL}	0.0025
Gain length L_{gain}	73.5 cm
Saturation length L_{sat}	8 m
X-ray parameters	
Wavelength λ_X	0.1 nm ($E_{\text{phton}} = 12.4$ keV)
Photon flux N_{photon}	4.4×10^{26} s^{-1}
Peak brilliance B_{peak}	$4.4\times10^{32}\left[\text{photons/s mm}^2\ \text{mrad}^2\ 0.1\%\text{BW}\right]$

Table 1. The design parameters of a table-top X-ray FEL driven by a laser-plasma-based accelerator.

4.2 A high-quality electron beam injector

4.2.1 Self-injection in the bubble regime

Most of LPA experiments that successfully demonstrated the production of quasi-monoenergetic electron beams with narrow energy spread have been elucidated in terms of self-injection and acceleration mechanism in the bubble regime (Kostyukov et al. 2004; Lu et al., 2006). In these experiments, electrons are self-injected into a nonlinear wake, often referred to as a bubble, i.e. a cavity void of plasma electrons consisting of a spherical ion column surrounded with a narrow electron sheath, formed behind the laser pulse instead of a periodic plasma wave in the linear regime. Plasma electrons radially expelled by the radiation pressure of the laser form a sheath with thickness of the order of the plasma skin depth c/ω_p outside the ion sphere remaining unshielded behind the laser pulse moving at relativistic velocity so that the cavity shape should be determined by balancing the Lorentz force of the ion sphere exerted on the electron sheath with the ponderomotive force of the laser pulse. This estimates the bubble radius R_B matched to the laser spot radius r_L, approximately as

$$k_p R_B \approx k_p r_L \approx 2\sqrt{a_0}\ , \tag{117}$$

for which a spherical shape of the bubble is created. This condition is reformulated as

$$a_0 \simeq 2\left(\frac{P}{P_c}\right)^{1/3}, \tag{118}$$

where $P_c \simeq 17(\omega_0^2/\omega_p^2)$ GW is the critical power for the relativistic self-focusing (Lu et al., 2006). The electromagnetic fields inside the bubble is obtained from the wake potential of the ion sphere moving at the velocity v_B as

$$\frac{eE_z}{mc\omega_p} = -\frac{1}{2}k_p\zeta\ , \text{and}\ \frac{eE_r}{mc\omega_p} = -\frac{1}{2}k_p r\ , \tag{119}$$

where $\zeta = z - v_B t$ is the coordinate in the moving frame of the bubble and r the radial coordinate with respect to the laser propagation axis (Kostyukov et al. 2004). One can see that the maximum accelerating field is given by $eE_{z\max} = mc^2 k_p^2 R_B/2$ at the back of the bubble and the focusing force is acting on an electron inside the bubble. Assuming the bubble phase velocity is given by

$$v_B \approx v_g - v_{\text{etch}} \approx c\left[1 - \left(\frac{1}{2}+1\right)\frac{\omega_p^2}{\omega_L^2}\right], \tag{120}$$

where $v_{\text{etch}} \approx c\omega_p^2/\omega_L^2$ is the velocity at which the laser front etches back due to the local pump depletion, the dephasing length leads to

$$L_{\text{dp}} \approx \frac{c}{c - v_B} R_B \approx \frac{2}{3}\frac{\omega_L^2}{\omega_p^2} R_B \approx \frac{2}{3}\frac{n_c}{n_p} R_B\ . \tag{121}$$

Hence the electron injected at the back of the bubble can be accelerated up to the energy

$$W \approx \frac{1}{2} eE_{z\max} L_{\mathrm{dp}} \approx \frac{1}{6} mc^2 \left(k_p R_B\right)^2 \left(\frac{\omega_L}{\omega_p}\right)^2 \approx \frac{2}{3} mc^2 a_0 \frac{n_c}{n_p} . \tag{122}$$

Using the matched bubble radius condition, the energy gain is approximately given by

$$W \approx mc^2 \left(\frac{P}{P_r}\right)^{1/3} \left(\frac{n_c}{n_p}\right)^{2/3} , \tag{123}$$

where $P_r = m^2 c^5 / e^2 \approx 8.72$ GW (Lu et al., 2007).

The 2D and 3D particle-in-cell simulations confirm that quasi-monoenergetic electron beams are produced due to self-injection of plasma electrons at the back of the bubble from the electron sheath outside the ion sphere as the laser intensity increases to the injection threshold. As expelled electrons flowing the sheath are initially decelerated backward in a front half of the bubble and then accelerated in a back half of it toward the propagation axis by the accelerating and focusing forces of the bubble ions, their trajectories concentrate at the back of the bubble to form a strong local density peak in the electron sheath and a spiky accelerating field. Eventually the electron is trapped into the bubble when its velocity reaches the group velocity v_g of the laser pulse. The trapping cross section (Kostyukov et al. 2004)

$$\sigma_{\mathrm{trapping}} \simeq \frac{2\pi}{k_p^3 d} \left(\ln \frac{k_p R_B}{\sqrt{8}}\right)^{-1} , \tag{124}$$

with the sheath width d imposes $k_p R_B \approx 2\sqrt{a_0} \geq \sqrt{8}$, i.e. $a_0 \geq 2$ for the matched bubble radius. Once an electron bunch is trapped in the bubble, loading of trapped electrons reduces the wakefield amplitude below the trapping threshold and stops further injection. Consequently the trapped electrons undergo acceleration and bunching process within a separatrix on the phase space of the bubble wakefield. This is a simple scenario for producing high-quality monoenergetic electron beams in the bubble regime.

However, in most of laser-plasma experiments aforementioned conditions and scenarios are not always fulfilled. In the experiment for the plasma density $n_p = (1-2) \times 10^{19}$ cm^{-3}, observation of the self-injection threshold on the normalized laser intensity gives $a_{0\mathrm{th}} \approx 3.2$ after accounting for self-focusing and self-compression that occur during laser pulse propagation in the plasma. In terms of the laser peak power

$$\frac{P}{P_c} = \frac{\pi^2}{8} \frac{a_0^2 r_L^2}{\lambda_p^2} , \tag{125}$$

the self-injection threshold for the power $(P / P_c)_{th} \approx 12.6$ as the laser spot size reduces to the plasma wavelength due to the relativistic self-focusing (Mangles et. al, 2007). In the

experiment at $n_p = (3-5)\times 10^{18}$ cm^{-3}, the self-injection threshold is $(P/P_c)_{\text{th}} = 3$, corresponding to $a_{0\text{th}} = 1.6$ (Froula et al., 2009).

4.2.2 A design example of self-injection bubble-regime LPA

We study the production of high-quality electron beams by means of the particle-in-cell (PIC) simulations for the self-injection. We have confirmed the qualities of accelerated electron beams with the r.m.s. energy spread less than 1%, the normalized transverse emittance of the order of a few π mm mrad and the r.m.s. bunch duration of the order of 1 fs. These parameters can satisfy the criteria of the electron beam injector that are required for X-ray FELs.

The self-injection electron beam production has been investigated by the 2D PIC simulation code VORPAL (Nieter et al., 2004), using the 2D moving window, of which the size is 83.5×120 μm^2 and the number of simulation cells is 1472×320, assuming H^+ immobile ions and 4 electrons per simulation cells. The laser pulse of the wavelength $\lambda_L = 0.8$ μm is focused on a spot size $r_L = 20$ μm, so that the peak normalized vector potential becomes $a_0 = 3$. Initially the laser pulse is located at $z = 0$ mm and after approximately $t = 1.7$ ps, it moves at the focal point $z = 0.5$ mm distant from the plasma edge. The transverse electron density forms a parabolic radial profile, given by Eq. (114). In this simulation, we set the on-axis plasma density and the density depth to be $n_p = 2\times 10^{18}$ cm^{-3} and $\Delta n = 0.3 n_p$, respectively. The longitudinal electron density and H^+ ion density of the plasma increase along with laser propagating axis from $z = 0$ mm to $z = 0.5$ mm and are constant over the rest of the simulation distance. The simulation has been carried out for the FWHM pulse duration $\tau_L = 27$, 35, 38, and 40 fs. For each pulse duration, two bunches are trapped and accelerated as follows: the higher energy bunch with narrow energy spread is trapped and accelerated in the first bucket of the wake, while the lower energy bunch with large energy spread is trapped to the second bucket of the wake. Figure 2 shows the energy spectrum of accelerated electron bunch for $\tau_L = 38$ fs at $z = 2.9$ mm, where the first bunch reaches the maximum energy and the minimum energy spread.

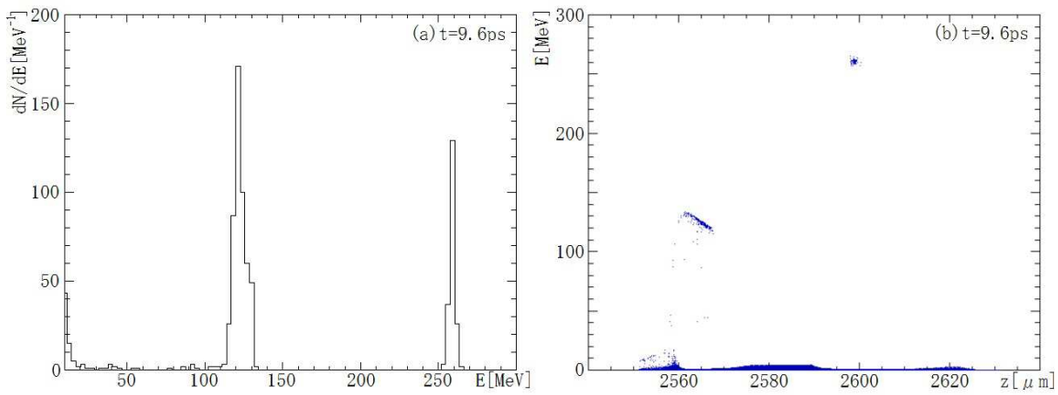

Fig. 2. The 2D PIC simulation results of the self-injected laser wakefield acceleration in the plasma channel for $a_0 = 3$, $\tau_L = 38$ fs, $r_L = 20$ μm, $n_p = 2\times 10^{18}$ cm^{-3} and $\Delta n_c = 0.3 n_p$: (a) the energy spectrum and (b) the phase space distribution of accelerated electrons at $t = 9.6$ ps.

The beam parameters such as the bunch energy, the energy spread, the charge, the normalized emittance and the bunch length of the first bucket are investigated as a function of the laser pulse duration, when the bunch energy reaches the maximum value, for which the bunch has travelled approximately the dephasing length. For the optimum pulse duration, we obtains the best beam parameters characterized by the energy $E_b = 283$ MeV, the r.m.s. relative energy spread $\sigma_E / E_b = 0.5$ %, the normalized emittance $\varepsilon_n = 2.2\pi$mm mrad, the r.m.s. bunch length $\sigma_b = 0.38$ μm (1.3 fs) and the peak beam current $I_b = 15$ kA, when a drive laser pulse with the peak power $P_L = 120$ TW ($a_0 = 3$) and pulse duration $\tau_L = 38$ fs is focused at the spot radius $r_L = 20$ μm into the entrance of the plasma channel with the channel depth $\Delta n / n_p = 0.3$. These electron beam parameters satisfy requirements for the table-top soft X-ray FEL capable of generating a 10 GW-class saturation power at the radiation wavelength of 13.5 nm (92 eV photon energy) using a 1.1-m long undulator with 5-mm period and the 1-Tesla magnetic field that give the undulator parameter $K_u = 0.465$ (Nakajima, 2011).

In practical applications, high-quality beams from laser-plasma injectors are transported and injected to the undulator or the next LPA stage through a beam transport system. We consider the compact beam transport system for focusing the above-mentioned accelerated electron beam into the next accelerator stage or the miniature undulator for the soft X-ray FEL. The design has been studied using TRACE3D (Crandall & Rusthoi, 1997), which is an envelope code based on a first-order matrix description of the transport. The focus system consists of four permanent-magnet-based quadrupoles (PMQs), arranged in the defocus-defocus-focus-focus lattice configuration. The simulation results of TRACE3D are shown in Fig. 3, where the electron bunch is transported from the left to the right for the aforementioned beam parameters.

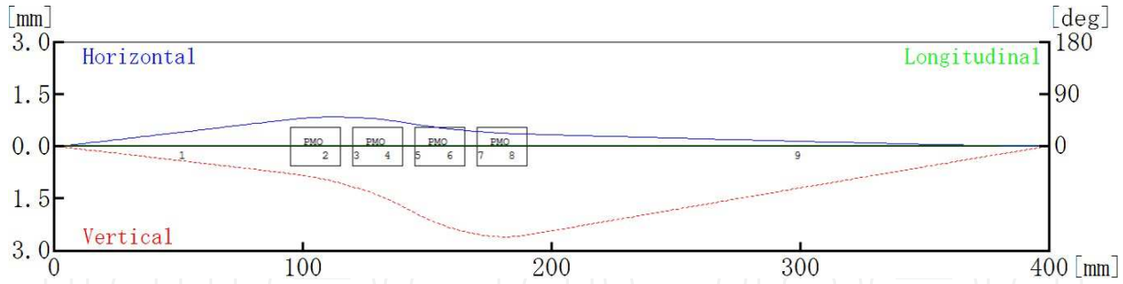

Fig. 3. TRACE3D simulation result of the electron beam transporting through the PMQ focus system for the beam energy $E_b = 283$ MeV, the normalized emittance $\varepsilon_{nx} = \varepsilon_{ny} = 2.2\pi$mm mrad, the relative energy spread $\sigma_E / E_b = 0.5$ %, the bunch duration $\sigma_{\tau b} = 1.3$ fs and the beam current $I_b = 15$ kA.

The field gradient of the two dimensional Halbach-type PMQ (Lim et al., 2005) is given by

$$B' = 2B_r \left(\frac{1}{r_i} - \frac{1}{r_0} \right), \tag{126}$$

where B_r is the tip field strength, r_i is the bore radius and r_0 is the outer radius of the PMQ. With $B_r = 2$ T and $r_i = 3$ mm, and $r_0 = 12$ mm, we can obtain the field gradient

$B' = 500$ T/m . In this simulation, we assume the parameters of the PMQs as follows: for PMQ1 and PMQ2, the field gradient $B' = -600$ T/m and for PMQ3 and PMQ4, $B' = 500$ T/m . All PMQs have the same permanent-magnet geometry, i.e. $r_i = 3$ mm , $r_0 = 12$ mm and the length of 20 mm. Since the electron beam only with the energy $E_b = 283$ MeV from the LPA located at the position $z = 0$ mm focuses on the horizontal and vertical r.m.s. beam sizes of $\sigma_x = 5.6$ μm and $\sigma_y = 6.9$ μm , respectively, at the position $z = 400$ mm , the second bunch with the lower energy $E_b \approx 120$ MeV and the larger energy spread overfocuses on the plane at $z = 400$ mm . Hence, we can tune the beam energy of the focus system so as to discriminate the first bunch with high energy and high qualities from the second bunch with low energy and less qualities.

5. Stability control of laser-plasma acceleration

Many of applications require the stability of the beam parameters as well as their qualities. In particular, the stability issue is crucial for the X-ray FEL relying on the SASE mechanism. The stability of the laser system itself is very important for achieving stable LPAs (Hafz et al., 2008). However, up to date there is no conclusive proposal for stabilizing the production of electron beams from LPAs at the low plasma densities which are relevant to GeV energies. Here we show the effect of laser pulse skewness (asymmetry) on minimizing the electron beam pointing angle in the weakly-nonlinear laser wakefield accelerator operating at the low densities in a gas jet target.

5.1 Experiment for stabilizing electron beam production

5.1.1 Setup and parameters

The experimental setup is described as follows. A laser beam from a titanium sapphire system had, after compressor, the energy of ~ 0.9 J per pulse. The laser pulses are delivered to a target chamber and focused above a 4-mm long supersonic helium gas jet by using a focusing optic having F-number of 22 that focuses the laser pulse on the FWHM spot size $w_0 \approx 23 \pm 1$ μm in vacuum. The gas jet stagnation pressure is ~ 1 bar and the laser is focused at the height of a few millimeters above the nozzle, where the gas density is in the range of $10^{17} - 10^{18}$ cm^{-3} . Therefore the expected wavelength of the wakefield is in the range $\lambda_p \approx 30 - 100$ μm . The electron beam pointing angle is detected by using a LANEX Kodak phosphor screen which is located at the distance of 78.5 cm from the gas jet. The LANEX is imaged onto an intensified charge-coupled device located near the interaction chamber in a radiation shielded area (Hafz et al., 2008). In order to obtain temporally-asymmetric laser pulses, the distance between two gratings of the pulse compressor is detuned from its optimum value which produces the shortest (37 fs) and symmetric pulses. The temporal pulse shape is measured by using a spectral phase interferometer for direct electric field reconstruction (SPIDER) device. Of interest is the negative detuning (positive chirp) which produces fast rise time laser pulses. Through negative detuning values from 0 to 250 μm, the laser pulse asymmetry increases and its length increases from 37 fs to 74 fs. In this range, the laser intensity is in the range $7.5 \times 10^{17} - 1.46 \times 10^{18}$ W/cm^2 , corresponding to the normalized vector potential of the laser pulse in the range $a_0 = 0.59 - 0.83$. Therefore, this experiment is characterized roughly with the parameters $a_0 \le 1$ and $c\tau_L \le w_0 < \lambda_p$.

5.1.2 Results

In the following, the reference direction for the electron beam pointing angle is the laser beam direction itself. At first, we set the laser compression to optimum (no detuning), so that the laser intensity is $\sim 1.46\times10^{18}$ W/cm^2 . The helium gas jet backing pressure is 1 bar and the interaction point is located at 1 mm height to the nozzle. At this height the gas density is $\sim 1\times10^{18}$ cm^{-3} . With those interaction conditions, the probability of observing an electron beam is as low as 1% or lower. However, the situation dramatically changes by detuning the compressor grating distance toward negative values. At a detuning distance of -100 μm the electron beam started to appear, however, the beam pointing angle is as large as ± 40 mrad. (The ± sign here means the direction of deflection angle with respect to the laser reference. In what follows we will remove the ± sign for simplicity). By changing the detuning distance to –200 μm the electron beam pointing angle is improved to 25 mrad and to 15 mrad at the detuning of –300 μm. Then the electron beam pointing angle has increased again to 25 mrad by increasing the detuning to –500 μm. In this experiment, the electron beam pointing in the vertical direction is smaller than that in the horizontal one. At laser height of 1.75 mm to the nozzle position, we notice that the electron beam pointing angle is improved to 8.5 and 10 mrad for the detuning distances of –200 and –400 μm. The electron beam pointing angle (horizontally and vertically) has been dramatically reduced to 2 mrad at a laser height of 3.25 mm where the gas density is in the range of 10^{17} cm^{-3} . Each data point is an average of 10 successive shots. From these data we can conclude that a detuning distance of –200 through –250 μm and the height of 3.25 mm are almost the optimum conditions for producing the smallest electron beam pointing angles. It should be noted that for this detuning range the laser intensity is in the range of $7.5\sim9\times10^{17}$ W/cm^2 . More precise scanning for the grating detuning distance at a fixed laser height of 3.25 mm shows an interesting result as illustrated in Fig. 4. For this height and at zero detuning, the electron beam pointing angle is severely large ~100 mrad and the beam generation reproducibility is ~50%. Again, within the grating detuning range from –200 to –300 μm the electron beam pointing angle reaches its minimum value at 2 mrad. In addition, the electron generation reproducibility is almost 100%, and the electron beam charge is ~30 ±10 pC as measured by an integrating current transformer. The data points of Fig. 4 are averages over hundreds of successive laser shots except for those at 0 or positive detuning values where the electron beam production is null or extremely rare.

Finally, we measured the electron beam energy by using a bending dipole magnet (H-shaped) which had a uniform magnetic field intensity of 0.94 Tesla and a longitudinal length of 20 cm (Hafz et al., 2008). The distance from the gas jet to the magnet entrance is ~1.5 m and the LANEX is located at 25 cm from the end of the magnet. Between the gas jet and magnet we installed 1-m long helical undulator with 0.5 T magnetic field and 2.4 cm period for generating a synchrotron radiation. The distance from the gas jet to the undulator is 30 cm, and the inner diameter of the undulator tube is 9 mm. Thus an electron beam from the gas jet must enter the undulator, propagate through it and then enter the dipole magnet region which bends the beam into the LANEX screen. The measured electron beam have a quasi-monoenergetic energy peak at ~ 165 MeV. This article is focused on minimizing the fluctuation of the electron beam pointing angle, thus our results are crucial for on-going

world-wide experiments on compact free-electron laser and undulator radiation using intense laser irradiated gas jets as a compact electron beam accelerator (Hafz et al., 2010; Nakajima, 2008).

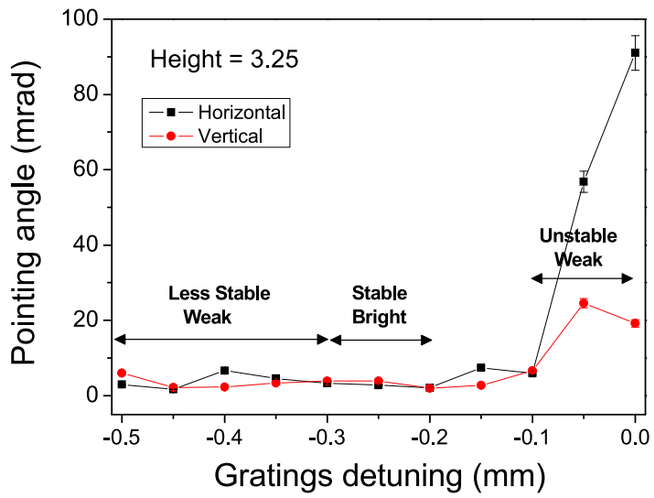

Fig. 4. Electron beam pointing angle versus detuning distance at the optimum height of 3.25 mm above the gas jet nozzle.

6. Conclusion

We have worked out the design considerations of a compact X-ray FEL that can reach the wavelength of 0.1 nm corresponding to the hard X-ray with photon energy of 12 keV. The system consists of a cm-scale 100 MeV-class electron beam injector, a 0.4-m long PMQ-based transport beam line , a 0.4-m long 6 GeV LPA linac and a 8-m long undulator. Including a 100 TW-class table-top laser system and an application space for the coherent X-ray research, main system can be installed within a 10-m long, 2-m wide space. The present considerations are based on the current achievements of laser-plasma accelerators and currently available technologies on drive lasers and undulators, for which we have not assumed new technologies and developments as well as new physics concepts on FEL. In this context, the present design of the hard X-ray FEL would be rather conventional and therefore it may be materialized in a near term at a reasonably low cost, guaranteeing the performance comparable to large-scale X-ray FELs. Harnessing miniature undulators with period of $\lambda_u \sim 5$ mm (Grüner et al., 2007; Eichner et al., 2007) may make the required saturation length shorter by a factor of 3, i.e. a 2.5-m long undulator, and the required electron beam energy becomes approximately half, i.e. $E_b = 3$ GeV , for a 0.1 nm X-ray wavelength, assuming the saturation length scales as $L_{\mathrm{sat}} \propto \lambda_u^{5/6}$ with $\gamma \propto \lambda_u^{1/2}$ and the LPA is operated at the same plasma density. This option may turn out a whole system to be on a 3-m long table top under the condition of trading off requirements for further high-quality, high-stability electron beam production from the LPAs.

Another way to build X-ray FELs on a table top is to produce the interaction between an electron beam and a laser pulse via coherent Thomson scattering or Compton scattering

(Bonifacio, 2005; Smetanin & Nakajima, 2004), where intense laser fields are used as an optical undulator or a laser wiggler/undulator that replaces the magnetic undulator field to the laser field with 3~4 orders magnitude shorter wavelength. Combining laser-plasma accelerated electron beams with laser undulators leads to further compact X-ray FELs, which have been recently proposed as all-optical-free electron lasers (Petrillo et al, 2008). However, these options must satisfy harsh requirements in terms of beam current, emittance, energy spread and stability of both laser and electron beams. We would like to expect further research and future progress in this new approach to a compact X-ray FEL using laser-plasma accelerators.

7. Acknowledgment

The work has been supported by the National Natural Science Foundation of China (Project Nos. 10834008, 60921004 and 11175119) and the 973 Program (Project No. 2011CB808104). K. Nakajima is supported by Chinese Academy of Sciences Visiting Professorship for Senior International Scientists.

8. References

Ackermann, W., Asova, G., Ayvazyan, Y. et al., Operation of a free-electron laser from the extreme ultraviolet to the water window. *Nature Photonics*, Vol. 1, No. 6, (June 2007), pp. 336 – 342, ISSN 1749-48852007

Bonifacio, R., Pellegrini, C., Narducci, L.M. (1984). Collective instabilities and high-gain regime in a free electron laser. *Optics Communications*, Vol. 50, No. 6, (July 1984), pp. 373-378

Bonifacio, R. (2005). Quantum SASE FEL with laser wiggler. *Nuclear Instruments and Methods in Physics Research A*, Vol. 546, pp. 634-638

Clayton, C.E., Ralph, J.E., Albert, F., Fonseca, R.A., Glenzer, S.H., Joshi, C., Lu, W., Marsh, K. A., Martins, S. F., Mori, W.B., Pak, A., Tsung, F.S., Pollock, B.B., Ross, J.S., Silva, L.O. & Froula, D. H. (2010). Self-guided laser wakefield acceleration beyond 1 GeV using ionization-induced injection. *Physical Review Letters*, Vol. 105, pp. 105003-1-4

Crandall, K., & Rusthoi, D. (1997). *TRACE 3-D documentation* (Third Edition), Los Alamos National Laboratory Technical Report No. LA-UR-97-886, Los Alamos National Laboratory, Los Alamos, New Mexico 87545

Eichner, T., Grüner, F., Becker, S., Fuchs, M., Habs, D., Weingartner, R., Schramm, U., Backe, H. (2007). Miniature magnetic devices for laser-based, table-top free-electron lasers. *Physical Review Special Topics - Accelerators and Beams*, Vol. 10, pp. 082401-1-9

Esarey, E., Sprangle, P., Krall, J., & Ting, A. (1996). Overview of plasma-based accelerator concepts. *IEEE Transactions on Plasma Science*, Vol. 24, No. 2, (April 1996), pp. 252-288

Froula, D.H., Clayton, C.E., Döppner, T., Marsh, K.A., Barty, C.P.J., Divol, L., Fonseca, R.A., Glenzer, S.H., Joshi, C., Lu, W., Martins, S.F., Michel, P., Mori, W.B., Palastro, J.P., Pollock, B.B., Pak, A., Ralph, J.E., Ross, J.S., Siders, C.W., Silva, L.O., & Wang, T. (2009) Measurements of the critical power for self-injection of electrons in a laser wakefield accelerator, *Physical Review Letters*, Vol. 103, pp. 215006-1-4.

Fuchs, M., Weingartner, R., Popp, A., Major, Zs., Becker, S., Osterhoff, J., Cortrie, I., Benno Zeitler, B., Rainer Hörlein, R., Tsakiris, G.D., Schramm, U., Rowlands-Rees, T.P., M. Hooker, S.M., Habs, D., Krausz, F., Karsch, S., & Grüner, F. (2009). Laser-driven soft-X-ray undulator source, *Nature Phys*. Vol. 5, pp. 826 – 829, ISSN 1745-2473

Gerstner, E. (2011). Free Electron Lasers - X-ray crystallography goes viral. *Nature Physics*, Vol. 7, No. 3, (March 2011), pp. 194-194, ISSN 1745-2473

Grüner, F., Becker, S., Schramm, U., Eichner, T., Fuchs, M., Weingartner, R., Habs, D., Meyer-Ter-Vehn., J., Geissler, M., Ferrario, M., Serafini, L., Van der Geer, B., Backe, H., Lauth W., & Reiche, S. (2007). Design considerations for table-top, laser-based VUV and X-ray free electron lasers. *Applied Physics B*, Vol. 86, pp. 431-435

Hafz, N.A.M., Jeong, T.M., Choi, I.W., Lee, S.K., Pae, K.H., Kulagin, V.K., Sung, J.H., Yu, T.J., Hong, K.H., Hosokai, T., R. Cary, J.R., Ko, D.K., & Lee, J.M. (2008). Stable generation of GeV-class electron beams from self-guided laser–plasma channels. *Nature Photonics*, Vol. 2, No. 9, (September 2008), pp. 571 – 577, ISSN 1749-4885

Hafz, N.A.M., Yu, T.J., Lee, S.K., Jeong, T.M., Sung, J.H., & Lee, J.M. (2010). Controlling the Pointing angle of a relativistic electron beam in a weakly-nonlinear laser wakefield accelerator. *Applied Physics Express*, Vol. 3, pp. 076401-1-3

Jackson, J. D. (1999). *Classical Electrodynamics* (Third Edition), Wiley, New York

Kameshima, T., Hong, W., Sugiyama, K., Wen, X.L., Wu, Y.C., Tang, C.M., Qihua Zhu, Q.H., Gu, Y.Q., Zhang, B.H., Peng, H.S., Kurokawa, S., Chen, Tajima, T., Kumita, T. & Nakajima, K. (2008). 0.56 GeV laser electron acceleration in ablative-capillary-discharge plasma channel. *Applied Physics Express*, Vol. 1, pp. 066001-1-3

Karsch, S., J Osterhoff, J., Popp, A., Rowlands-Rees, T.P., Major, Zs., Z M Fuchs, Z.M., Marx, B., Hörlein, R., K Schmid, K., Veisz, L., Becker, S., Schramm, U., Hidding, B., Pretzler, G., Habs, D., Grüner, F., Kraus, F., & S M Hooker, S.M. (2007). GeV-scale electron acceleration in a gas-filled capillary discharge waveguide. *New Journal of Physics,* Vol. 9, pp. 415-425

Kostyukov, I., Pukhov, A., Kiselev, S. (2004). Phenomenological theory of laser-plasma interaction in "bubble" regime. *Physics of Plasmas*, Vol. 11, pp. 5256-5264

Leemans, W.P., Nagler, B., Gonsalves, A.J., Toth, Cs., Nakamura, K., Geddes, C.G.R., Esarey, E., Schroeder, C.B. & Hooker, S.M. (2006). GeV electron beams from a centimetre-scale accelerator. *Nature Physics*, Vol. 2, pp. 696-699, ISSN 1745-2473

Lim, J.K., Frigola, P., Travish, G., Rosenzweig, J.B., Anderson, S.G., Brown, W.J., Jacob, J.S., Robbins, C.L., & Tremaine, A.M. (2005). Adjustable short focal length permanent-magnet quadrupole based electron beam final focus system. *Physical Review Special Topics - Accelerators and Beams*, Vol. 8, pp. 072401-1-17

Lu, H.Y., Liu, M.W., Wang, W.T., Wang, C., Liu, J.S., Deng, A.H., Xu, J.C., Xia, C.Q., Li, W.T., Zhang, H., Lu, X.M., Wang, C., Wang, J.Z., Liang, X.Y., Leng, Y.X., Shen, B.F., Nakajima, K., Li, R.X. & Xu, Z.Z. (2011). Laser wakefield acceleration of electron beams beyond 1 GeV from an ablative capillary discharge waveguide. *Applied Physics Letters*, Vol. 99, pp. 091502-1-3

Lundh, O., Lim, J., C. Rechatin1, Ammoura, L., Ben-Ismaïl, A., Davoine, X., Gallot, G., Goddet, J-P., Lefebvre, E., Malka, V. & Faure, J. (2011). Few femtosecond, few kiloampere electron bunch produced by a laser–plasma accelerator. *Nature Physics*, Vol. 7, No. 3, (March 2011), pp. 219-222, ISSN 1745-2473

Lu, W., Huang, C., Zhou, M., Mori, W.B. & Katsouleas, T. (2006). Nonlinear theory for relativistic plasmawakefields in the blowout regime. *Physical Review Letters*, Vol. 96, pp. 165002-1-4

Lu, W., Tzoufras, M., Joshi, C., Tsung, F.S., Mori, W.B., Vieira, J., Fonseca, R.A., & L. O. Silva, L.O. (2007). Generating multi-GeV electron bunches using single stage laser wakefield acceleration in a 3D nonlinear regime. *Physical Review Special Topics - Accelerators and Beams*, Vol. 10, pp. 061301-1~12

Malka, V., Faure, J., Gauduel, Y.A., Lefebvre, E., Rousse, A., & Phuoc, K.T. (2008). Principles and applications of compact laser–plasma accelerators. *Nature Physics*, Vol. 4, No. 6, (June 2008), pp. 447-453, ISSN 1745-2473

Mangles, S.P.D., Thomas, A.G.R., Lundh, O., Lindau, F., Kaluzac, M. C., Persson, A., Wahlström, C.-G., Krushelnickd, K., & Najmudin, Z., (2007). On the stability of laser wakefield electron accelerators in the monoenergetic regime, *Physics of Plasmas*, Vol. 14, pp. 056702-1~7.

Michel, P., Schroeder, C.B., Shadwick, B.A., Esarey, E. & Leemans, W.P. (2006). Radiative damping and electron beam dynamics in plasma-based accelerators. *Physical Review E* , Vol. 74, pp. 026501-1-14

Nakajima, K. (2008). Compact X-ray sources-Towards a table-top free-electron laser. *Nature Physics*, Vol. 4, No. 2, (February 2008), pp. 92-93, ISSN 1745-2473

Nakajima, K. (2011). Recent Progress on Laser Plasma Accelerators and Applications for Compact High-Quality Particle Beam and Radiation Sources, *Journal of Materials Science and Engineering A*, Vol. 1, pp. 293-300, ISSN 1934-8959

Nakajima, K., Kando, M., Kawakubo, T., Nakanishi, T., & Ogata, A. (1996). A table-top X-ray FEL based on the laser wakefield accelerator-undulator system. *Nuclear Instruments and Methods in Physics Research*, Vol. A375, pp. 593-596

Nakajima, K., Deng, A., Zhang, X., Shen, B., Liu, J., Li, R., Xu, Z., Ostermayr, T., Petrovics, S., Klier, C., Iqbal, K., Ruhl, H. & Tajima, T. (2011). Operating plasma density issues on large-scale laser-plasma accelerators toward high-energy frontier. *Physical Review Special Topics - Accelerators and Beams*, Vol. 14, pp. 091301-1-12

Nieter, C. & Cary, J.R. (2004) VORPAL: a versatile plasma simulation code. *Journal of Computational Physics*, Vol. 196, No. 2, pp. 448-473

Osterhoff, J., Popp, A., Major, Zs., Marx, B., Rowlands-Rees, T.P., Fuchs, M., Geissler, M., Hörlein, R., Hidding, B., Becker, S., Peralta, E.A., Schramm, U., Grüner, F., Habs, D., Krausz, F., Hooker, S.M., & Karsch, S. (2008). Generation of stable, low-divergence electron beams by laser-wakefield acceleration in a steady-state-flow gas cell. *Physical Review Letters*, Vol. 101, pp. 085002-1-4

Petrillo, V., Serafini, L., & Tomassini1, P. (2008). Ultrahigh brightness electron beams by plasma-based injectors for driving all-optical free-electron lasers. *Physical Review Special Topics - Accelerators and Beams*, Vol. 11, pp. 070703-1-7

Rechatin, C., Faure, J., Ben-Ismail, A., Lim, J., Fitour, R., Specka, A., Videau, H., Tafzi, A., Burgy, F., & Malka, V. (2009). Controlling the phase-space volume of injected electrons in a laser-plasma accelerator. *Physical Review Letters,* Vol. 102, pp. 164801-1-4

Schachter, L. (2011). *Beam-Wave Interaction in Periodic and Quasi-Periodic Structures* (Second Edition), Springer-Verlag, ISBN 978-3-642-19847-2, Berlin

Schlenvoigt, H.-P., Haupt, K., Debus, A., Budde, F., Jackel, O., Pfotenhauer, S., Schwoerer, H., Rohwer, E., Gallacher, J.G., Brunetti, E., Shanks, R.P., Wiggins, S.M., & Jaroszynski, D.A. (2008). A compact synchrotron radiation source driven by a laser-plasma wakefield accelerator. *Nature Physics*, Vol. 4, No. 2, (February 2008), pp. 130-133, ISSN 1745-2473

Sprangle, P., & Esarey, E. (1992). Interaction of ultrahigh laser fields with beams and plasmas. *Physics Fluids B*, Vol.4, No. 7, (July 1992), pp. 2241-2248

Smetanin, I.V., & Nakajima, K. (2004). Quantum effects in laser-beam Compton interaction and stimulated electron positron annihilation in a strong field. *Laser and Particle Beams*, Vol. 22, pp. 479-484

Sverto, O. (1998). *Principles of Lasers* (Fourth Edition), Plenum Press, ISBN 0-306-45748-2, New York

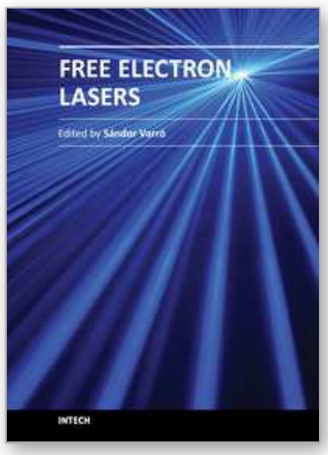

Free Electron Lasers

Edited by Dr. Sandor Varro

ISBN 978-953-51-0279-3
Hard cover, 250 pages
Publisher InTech
Published online 14, March, 2012
Published in print edition March, 2012

Free Electron Lasers consists of 10 chapters, which refer to fundamentals and design of various free electron laser systems, from the infrared to the xuv wavelength regimes. In addition to making a comparison with conventional lasers, a couple of special topics concerning near-field and cavity electrodynamics, compact and table-top arrangements and strong radiation induced exotic states of matter are analyzed as well. The control and diagnostics of such devices and radiation safety issues are also discussed. Free Electron Lasers provides a selection of research results on these special sources of radiation, concerning basic principles, applications and some interesting new ideas of current interest.

How to reference

In order to correctly reference this scholarly work, feel free to copy and paste the following:

Kazuhisa Nakajima, Aihua Deng, Hitoshi Yoshitama, Nasr A. M. Hafz, Haiyang Lu, Baifei Shen, Jiansheng Liu, Ruxin Li and Zhizhan Xu (2012). Laser-Driven Table-Top X-Ray FEL, Free Electron Lasers, Dr. Sandor Varro (Ed.), ISBN: 978-953-51-0279-3, InTech, Available from: http://www.intechopen.com/books/free-electron-lasers/laser-driven-table-top-x-ray-fel

INTECH
open science | open minds

InTech Europe
University Campus STeP Ri
Slavka Krautzeka 83/A
51000 Rijeka, Croatia
Phone: +385 (51) 770 447
Fax: +385 (51) 686 166
www.intechopen.com

InTech China
Unit 405, Office Block, Hotel Equatorial Shanghai
No.65, Yan An Road (West), Shanghai, 200040, China
中国上海市延安西路65号上海国际贵都大饭店办公楼405单元
Phone: +86-21-62489820
Fax: +86-21-62489821

IntechOpen